Hydrol. Earth Syst. Sci. Discuss., 12, 3787–3846, 2015
www.hydrol-earth-syst-sci-discuss.net/12/3787/2015/
doi:10.5194/hessd-12-3787-2015

Hydrology and Earth System Sciences
Open Access
Discussions

Stochastic approach to analyzing the uncertainties and possible changes in the availability of water in the future based on a climate change scenario

G. G. Oliveira, O. C. Pedrollo, and N. M. R. Castro

Institute of Hydraulic Research – Federal University of Rio Grande do Sul, Porto Alegre, RS, Brasil

Received: 11 December 2014 – Accepted: 20 March 2015 – Published: 10 April 2015

Correspondence to: G. G. Oliveira (g.g.oliveira10@gmail.com)

Published by Copernicus Publications on behalf of the European Geosciences Union.

Abstract

The objective of this study was to analyze the changes and uncertainties related to water availability in the future (for purposes of this study, it was adopted the period between 2011 and 2040), using a stochastic approach, taking as reference a climate projection from the climate model Eta CPTEC/HadCM3. The study was applied to the Ijuí river basin in the south of Brazil. The set of methods adopted involved, among others, correcting the climatic variables projected for the future, hydrological simulation using Artificial Neural Networks to define a number of monthly flows and stochastic modeling to generate 1000 hydrological series with equal probability of occurrence. A multiplicative type stochastic model was developed in which monthly flow is the result of the product of four components: (i) long term trend component; (ii) cyclic or seasonal component; (iii) time dependency component; (iv) random component. In general the results showed a trend to increased flows. The mean flow for a long period, for instance, presented an alteration from 141.6 (1961–1990) to 200.3 $m^3 s^{-1}$ (2011–2040). An increment in mean flow and in the monthly SD was also observed between the months of January and October. Between the months of February and June, the percentage of mean monthly flow increase was more marked, surpassing the 100 % index. Considering the confidence intervals in the flow estimates for the future, it can be concluded that there is a tendency to increase the hydrological variability during the period between 2011–2040, which indicates the possibility of occurrence of time series with more marked periods of droughts and floods.

1 Introduction

Discussions concerning variability and climate changes have intensified in the last few decades. Many studies have proved significant alterations in the composition of the atmosphere and, consequently, in the climate-related variables. On this topic the IPCC (Intergovernmental Panel on Climate Changes) should be highlighted. It was estab-

HESSD
12, 3787–3846, 2015

lished in 1988 by the World Meteorological Organization (WMO) and by the United Nations Environment Program (UNEP) whose objective is to supply scientific information in order to gain a better understanding of changes in the global climate, so as to evaluate their impact on society and on nature, and propose alternatives for adaptation and mitigation.

According to IPCC (2013), it is already clear that the Earth is warming, as proved by the rise in the mean temperatures of the air and the oceans, by the increase in the mean level of the seas and by the acceleration of ice melt in mountain or polar climate regions. Studies developed on a global scale have shown that several natural systems are already under the impact of climate changes.

Changes in temperature and precipitation will lead to an increased frequency of extreme meteorological events, such as severe floods and droughts, which will inevitably affect the availability of water for human consumption, irrigation, industries and other uses (IPCC, 2013). Some research studies on the sensitivity of agricultural crops to climate changes show that there may be a strong negative effect on crop growth, increasing the risk of losses in harvests worldwide (Mearns et al., 1996; Richter and Semenov, 2005; Zhang and Liu, 2005; Rasmussen et al., 2012).

The climate scenario projections are performed using Global Climate Models (GCMs) and Regional Climate Models (RCMs). The resolution of RCMs is between 10 and 50 km, which allow applying them in scenarios of climate changes in medium and small basins. Using these models, together with the GCMs, enables detailing the climate processes at the local level, detecting the variations and specificities of a given region, and thus improving the understanding of impacts in small basins (Marengo et al., 2009, 2012).

The Eta Model was developed at Belgrade University and operationally implemented by the National Centers for Environmental Prediction (Black, 1994). The vertical coordinate system used in this model is recommended for use over South America due to the presence of the Andes mountain range (Marengo et al., 2012). Recently, a new version

HESSD
12, 3787–3846, 2015

of Eta Model, Eta CPTEC, was developed independently by the National Institute for Space Research (INPE).

The regional Eta Model was configured over South America and applied to downscale HadCM3 members of the Perturbed Physics Ensemble (PPE) experiment for the present climate (1961–1990). The dynamic downscaling method was used to generate the climate scenarios (Chou et al., 2012). According to Mujumdar and Kumar (2013), the main advantage of dynamical downscaling over the statistical downscale method is its ability to capture the mesoscale non-linear effects and provide information for many climate variables, while ensuring internal consistency with respect to the physical principles in meteorology, simulating satisfactorily some regional climatic conditions.

The Eta CPTEC Model includes the increase in CO_2 concentration levels according to the scenario of emission and daily variation of the state of vegetation during the year. This model reproduces scenario A1B of IPCC SRES, supplied by the global coupled ocean–atmosphere HadCM3, in four members (versions) of disturbance in the global model – (no disturbance – CNTRL; low sensitivity – LOW; medium sensitivity – MID; high sensitivity – HIGH), which represent the uncertainty of boundary conditions, to produce variants of the same model (Chou et al., 2012; Marengo et al., 2012). The regional model was integrated into the horizontal resolution of 40 km, for the period between 1961 and 1990, and the future scenarios were generated in three 30 year periods (from 2011 to 2040, from 2041 to 2070, from 2071 to 2100) (Chou et al., 2012).

The study of Marengo et al. (2012) details the scenarios generated for South America using the Eta CPTEC/HadCM3 Model. According to this study, the model is configured with 38 vertical layers with the top of the model at 25 hPa. The Mellor–Yamada level 2.5 procedure (Mellor and Yamada, 1974) was used for the treatment of turbulence. The radiation package was developed by the Geophysical Fluid Dynamics Laboratory, based in studies of Fels and Schwarzkopf (1975) and Lacis and Hansen (1974). The Eta Model uses the Betts–Miller (Betts and Miller, 1986) scheme modified by Janjic (1994) to parameterize deep and shallow cumulus convection, and the Zhao scheme (Zhao et al., 1997) to parameterize cloud microphysics. This model uses

HESSD
12, 3787–3846, 2015

also the NOAH scheme (Ek et al., 2003) to parameterize the land–surface transfer processes (Marengo et al., 2012).

Pesquero (2009), Chou et al. (2012) and Marengo et al. (2012) used Model Eta CPTEC. In the first two studies, the model was used to reproduce the present climate on South America and certify the quality of the model. A smooth tendency was observed to underestimate precipitation over the Amazon in the rainy season and the central region of Brazil, in the Brazilian Savanna. In the last study (Marengo et al., 2012), model Eta CPTEC was used to study the climate changes in the Amazon, São Francisco and Paraná river basins between 2011 and 2100.

Currently, in the scientific literature, there are several studies that analyze the effects of climate changes on water availability (examples: Kleinn et al., 2005; Hughes et al., 2011; Gunawardhana and Kazama, 2012). On a continental or global scale, normally, the outputs of the GCMs are used in combination with the empirical macroscale hydrological models which perform the water balance (for instance, Arnell, 1999, 2004; Nijssen et al., 2001; Milly et al., 2005; Nohara et al., 2006). The studies on water availability in smaller river basins normally use the climate projections for the RCMs, associated with empirical or physically-based hydrological models, in a deterministic approach, offering only a single result in the hydrological sphere for each climate scenario. Examples of this are the studies by Middelkoop et al. (2001), Menzel and Bürger (2002) and Kleinn et al. (2005).

However, because of the randomness of hydrometeorological processes, the uncertainties related to climate modeling and future water availability favor the use of probabilistic methods based on stochastic time series, as in the studies by Wilks (1992), Semenov and Barrow (1997) and Booij (2005). The stochastic approach broadens the possibility of analyzing water availability and the climatic uncertainties in the future, offering a great number of scenarios for analysis, and it is possible to identify the confidence intervals in the projection and to estimate the random component of the climatic and hydrological dynamics.

HESSD
12, 3787–3846, 2015

However, when generating hundreds or thousands of stochastic climate series, it is necessary to repeat the hydrological simulation often, rendering the modeling process very onerous from the computational standpoint. Moreover, in this approach the hydrological scenarios produced become even more sensitive to any imprecision in estimating the parameters of the rainfall-flow transformation model.

In order to minimize the processing time, this methodology will cover the randomness of the processes and the climate dynamics directly in the flow series, using a stochastic model appropriate for monthly flows. Thus, based on a single climate scenario, a flow series is generated by hydrological deterministic simulation and then the stochastic process is performed.

The objective of this study is to analyze the possible scenarios and uncertainties related to water availability in future, using a stochastic approach based on a climatic change scenario originating in the Eta CPTEC/HadCM3 climate model. This study will be applied to the Ijuí river basin, in Rio Grande do Sul (RS), Brazil.

2 Methodology

The set of methods adopted in this study comprised the use of observed and simulated hydrometeorological data, to analyze the uncertainties and possible scenarios of water availability in the future, based on a climatic scenario originating in the regional climate model Eta CPTEC/HadCM3.

Simplifying, the methodological procedure covered: (i) spatial interpolation of the meteorological variables; (ii) selection of the climatic scenario and correction of the climate variables; (iii) estimation of the potential evapotranspiration; (iv) hydrological simulation using Artificial Neural Networks (ANNs); (v) stochastic modeling of monthly flows to generate possible hydrological series in the future.

For this study, considering the availability of the climatic data derived from the regional climate model Eta CPTEC/HadCM3 (provided by the National Institute for Space

HESSD
12, 3787–3846, 2015

Research – INPE), the years between 1961 and 1990 was considered as a base period and the years between 2011 and 2040 was considered as the "future" period.

2.1 Study Area

This study was applied in the Ijuí River Basin, in the Santo Ângelo stream gauging section, in the northwest of RS, Brazil. The basin area is 5414 km^2 and it is located between the following geographic coordinates: latitudes 27.98 to 28.74° S and longitudes 53.21 and 54.28° W (Fig. 1). At this stream gauging station between 1941 and 2005, the mean flow ($\overline{Q}$) was 138 $m^3 s^{-1}$, and the dry and high flow periods were the months of March ($\overline{Q}$ = 72 $m^3 s^{-1}$) and October ($\overline{Q}$ = 211 $m^3 s^{-1}$), respectively.

The area of the study was chosen because the region depends to a great extent on agricultural activities and may suffer serious socioeconomic impacts from the climate changes. According to the State Coordinator of Civil Defense of RS, during the period between 1982 and 2011 there were at least six severe dry periods in the basin region, which caused great losses to the agricultural and cattle activities, mainly those involving soy beans and maize.

Considering the daily climate data of the Cruz Alta station, operated by INMET (National Institute of Meteorology), the winter and spring months (from June to December) are the rainiest. According to Rossato (2011), annual mean precipitation oscillates between 1700 and 1800 mm, between 100 and 120 days of rain a year, on average. The annual mean temperature oscillates between 17 and 20 °C. The coldest months are June and July, with a mean of around 14 °C, and the warmest months are January and February, with a mean of around 24 °C.

2.2 Data

The following materials were used in this study: (i) daily historical series of precipitations provided by the HidroWeb site of the National Water Agency (ANA), during the period between 1961 and 1990, at 77 rain gauging stations within the radius of cover-

HESSD
12, 3787–3846, 2015

age of 100 km of the basins boundaries (Fig. 2); (ii) daily historical series of precipitation provided by IPH (Castro et al., 1999), in the years 1989 and 1990, at 22 rain gauging stations (Fig. 2); (iii) daily historical series of precipitation, temperature, wind speed, solar radiation, atmospheric pressure and relative humidity of the air provided through the portal of BDMEP (Bank of Meteorological Data for Teaching and Research) of INMET, during the period between 1961 and 1990, at five meteorological stations (Fig. 2); (iv) daily historical series of flows from the Santo Ângelo station, located at coordinates 28.36° S and 54.27° W, provided through the HidroWeb site, during the period between 1961 and 1990; (v) daily data simulated by the regional climate model Eta CPTEC, conducted by four members of the global climate model HadCM3, with different levels of sensitivity (CNTRL, LOW, MID and HIGH), during the periods of 1961–1990 (base) and 2011–2040 ("future"). The variables simulated were: precipitation, temperature, wind speed, relative humidity of the air, atmospheric pressure and solar radiation.

2.3 Spatial interpolation

The first stage consisted of the spatial interpolation of the five daily climate variables (temperature, wind speed, relative humidity of the air, atmospheric pressure and solar radiation), and daily precipitation in the periods between 1961–1990 (observed and simulated data) and 2011–2040 (data simulated by the Eta model). The interpolation grid was generated with a spatial resolution of 5 km (Fig. 2), totalizing 264 nodes in the basin area. The interpolation procedure was performed for all data sets: (i) series observed at 104 rain gauging or meteorological stations; (ii) series simulated using model Eta CPTEC/HadCM3 in four scenarios of climate sensitivity (CNTRL, LOW, MID and HIGH).

The use of so many stations in a 100 km radius, to begin the interpolation process consists of a safety margin, since many of these stations present short series, with many gaps. Thus, only on a few days when the stations closest to the interpolation grid present gaps, the method can select rainfall data from stations located slightly further away, in this way avoiding failures in estimating precipitation during the interpolation

HESSD
12, 3787–3846, 2015

process. It can be said that for each day, in every node of the interpolation grid, only the closest stations with rainfall data were used, usually within the basin and immediate surroundings.

The interpolation method used was that of the natural neighbor (Sibson, 1981). This interpolation method obtained the best results in the study presented by Silva et al. (2013), with precipitation series similar to those used in the present study, also in the Ijuí River basin. In the study mentioned, the following methods were also tested: closest neighbor, linear triangulation and inverse distance weighting.

The natural neighbor method is based on the concept of area of influence of the sampling points determined by Voronoi polygons. These polygons are obtained from the Delaunay triangulation. For each point on the interpolation grid, the weight of each sampling point is calculated because of the area of influence. The daily value of each variable in the basin was obtained from the mean of the values interpolated in all nodes of the regular grid.

Still at this stage, the daily mean value of the five climate variables and of precipitation in the Ijuí River basin was calculated, considering the data observed and the data simulated by the ETA model. Finally, the monthly accumulated precipitation for the observed series and for scenarios simulated by the Eta model in the periods of 1961–1990 (base) and 2011–2040 (future) were calculated.

2.4 Selection of climate scenario and correction of climate variables

The outputs of climate models should not be used directly to estimate future water availability (Graham, 2000). The climate models may not represent perfectly the current climate due mainly to the influence of the spatial discretization of the models. It is observed (Lenderink et al., 2007) that the outputs may present systematic errors. The correction of climate variables is intended to prevent that the errors intrinsic to the output of the climate models are propagated to the subsequent hydrologic modeling.

Recently several techniques to correct the climate variables resulting from the GCMs and RCMs were developed and compared (Themeßl et al., 2012). The use of distur-

HESSD
12, 3787–3846, 2015

bances (Delta Change Approach) in climate variables is a commonly used strategy to simulate the impacts of climate changes, obtained via global or regional climate models on water resources (Graham, 2004; Lenderink et al., 2007). The technique consists of using only the seasonal change foreseen between the current and future scenario, obtained with the climate model. This change is represented by the difference between the current climatic conditions and those foreseen for the future, both conditions obtained by the climate model. The change foreseen is incorporated to the historical series of precipitations and temperature to generate the series in the future. Thus the error associated with climate modeling is eliminated from the current conditions, and becomes limited to the uncertainties associated with the forecast of climate changes for the future. Examples of applying this methodology are the studies by Kaczmarek et al. (1996), Lettenmaier et al. (1999), Graham (2000), Bergström et al. (2001).

However, as mentioned by the authors themselves (Graham, 2000; Bergström et al., 2001), and supported by Lenderink et al. (2007), applying the forecast changes in temperature or in precipitation directly on the series observed implies considerable simplifications which may compromise the analysis of the projections in future. In this approach, for instance, probable changes in the number of rainy days, in dispersion (variance) of rains or in the extreme values of temperature are not considered, since the series itself observed in the past consists of the base of forecasts for the future, and only the seasonal mean variations are taken into account. In this case, there is a risk of considering that the same anomalies recorded in the past will be observed in the future with small changes in the monthly magnitude of climate variables, according to time of the year.

Thus, Lenderink et al. (2007) discuss and analyze how the output of a regional climate model should be corrected to obtain more realistic flows for the current climate and, consequently, for the future climate. According to the authors, the development of regional climate model, with some corrections in the output, allows the Direct Approach in using projections of temperature and rainfall for the future. This method, instead of adding the changes forecast in the series observed performs a different procedure:

HESSD
12, 3787–3846, 2015

(i) it detects the differences between the current climatic conditions, i.e., between the conditions observed using meteorological stations and the conditions simulated by the regional climate model; (ii) it applies these differences in the series forecast for the future.

Other more sophisticated methods have been tested and compared, with applications at daily or monthly time intervals, as can be seen in Wood et al. (2004), Maurer and Hidalgo (2008), Boé et al. (2007), Piani et al. (2010) and Bárdossy and Pegram (2011). In a recent study, Themeßl et al. (2011) compared a few correction methods and concluded that the Quantile-Based Mapping technique (Panofsky and Brier, 1968) is the most effective one to remove the errors in the precipitation data. This method is applied with small adaptations in the studies listed above. Essentially, the method is based on the differences between the accumulated probability curves (simulated and observed) of daily or monthly precipitations.

In the study by Oliveira et al. (2015a), whose objective was to evaluate the climatic conditions simulated using model Eta CPTEC/HadCM3, emphasizing the study of water availability in the Ijuí river basin, four methods to correct the climate variables were tested (Delta Change Approach, Direct Approach, Monthly Quantile-Based and Quarterly Quantile-Based). The control period in which the corrections were applied and the hydrological model calibrated, was defined between 1961 and 1975, and the evaluation period, in which the results of the climate scenarios and water availability were found was 1976 and 1990. For both periods data were available that had been observed at rain gauging stations and meteorological stations and data simulated by the regional climate model Eta CPTEC, conducted by four members of the global climate model HadCM3, with different levels of sensitivity.

The main results obtained in Oliveira et al. (2015a) were: (i) only Eta HIGH did not prove satisfactory in most of the aspects analyzed regarding precipitation, evapotranspiration, and flow; (ii) in evaluating the flows resulting from the hydrologic modeling process, the Eta LOW member was outstanding, especially as regards to the mean monthly flows (mean error of 22.6 %), to the annual flow permanence curves (mean er-

HESSD
12, 3787–3846, 2015

ror 12.6 %) and to the quarterly flow permanence curves (mean error 27.3 %); (iii) with Eta LOW a good adjustment can be seen, both to the low flows (permanence greater than 90 %) and to the high flows (permanence less than 10 %); (iv) the outstanding climate scenario was Eta LOW, applying the Direct Approach correction method, especially as to the curve of permanence of the flows; (v) finally, it was pointed out that in the case of the precipitations and flows the difference between simulated values, based on the Eta model and the values observed was greater than those of evapotranspiration, resulting in errors that were sometimes greater than 20 %. One should, therefore, consider that these uncertainties will be reproduced in future scenarios (for the coming decades of the 21st century).

Since the present study focuses on a stochastic approach that takes into account the uncertainties associated with the various stages that comprise the modeling of water availability in future, it was necessary to adopt a climate scenario to test the methodology. Thus, taking into account the results obtained in Oliveira et al. (2015a), the use of the Eta LOW member was defined, applying the Direct Approach correction method. In the Direct Approach method used by Lenderink et al. (2007), the precipitation that is corrected in the future period (2011–2040), in month k, in year j, is equal to the precipitation simulated during the same period, month and year, multiplied by a correction factor. The correction factor in this method is the ratio between the mean precipitation observed during the base period (1961–1990), in month k, and the mean precipitation simulated in the same period and month (Eq. 1).

$$P\mathrm{cor(fut)}_{k/j} = P\mathrm{sim(fut)}_{k/j} \times \left[\overline{P\mathrm{obs(base)}_k} / \overline{P\mathrm{sim(base)}_k}\right] \quad (1)$$

Where: $P\mathrm{sim(fut)}_{k/j}$ is the precipitation simulated during the future period, in month k and year j; $\overline{P\mathrm{obs(base)}_k}$ is the mean of the precipitation observed during the base period for month k; $\overline{P\mathrm{sim(base)}_k}$ is the mean of precipitation simulated during the base period for month k.

The other five climatic variables (temperature, wind speed, relative humidity of the air, atmospheric pressure and solar radiation) were corrected in the daily time interval,

HESSD
12, 3787–3846, 2015

using Direct Approach, as shown in Eq. (2).

$$C_Z\text{cor(fut)}_{i/k/j} = C_Z\text{sim(fut)}_{i/k/j} \times \left[\overline{C_Z\text{obs(base)}}_k / \overline{C_Z\text{sim(base)}}_k\right] \quad (2)$$

Where: $C_Z\text{cor(fut)}_{i/k/j}$ is the correct value of climate variable z in the future period, in day i, month k, and year j; $C_Z sim(fut)_{i/k/j}$ is the value simulated of climate variable z during the future period, in day i, month k, and year j; $\overline{C_Z\text{obs(base)}}_k$ is the mean value observed of the climate variable z during the base period for month k; $\overline{C_Z\text{sim(base)}}_k$ is the mean value simulated of the climate variable z during the base period for month k.

2.5 Estimation of reference evapotranspiration

In the third stage the (daily) reference evapotranspiration was calculated for the simulated and corrected climate scenario and for the observed series in the base (1961–1990) and future (2011–2040) periods. The reference evapotranspiration was calculated using the Penman–Monteith method (Penman, 1948; Monteith, 1965), which has been considered the most reliable method by some authors and was adopted as the standard method by the United National Food and Agriculture Organization (FAO) (Allen et al., 1998). This method is parameterized for an area completely covered with 12 cm high grass, considering the aerodynamic resistance of the surface of 70 s m^{-1} and albedo of 0.23, in soil without a water deficit.

After calculating the daily evapotranspiration, these values were converted to the monthly time interval, rendering it compatible with the monthly accumulated precipitation series for hydrological modeling.

2.6 Hydrological simulation using Artificial Neural Networks (ANNs)

Recently, several studies have obtained excellent results applying ANNs in the field of water resources and hydrology, especially in the development of models for simulation,

HESSD
12, 3787–3846, 2015

forecasting and classification (Bowden et al., 2005; Jain and Kumar, 2007; Leahy et al., 2008).

The methodology adopted in this study comprised the use of a hydrological model based on ANNs, consisting of transformations of the meteorological and pluviometric variables. The program for the necessary implementation was developed in the MATLAB R2010a environment, consisting mainly of a generalized model, constituted by linear transformations of inputs and outputs from a neural network with a hidden layer (Eq. 3).

$$\frac{(y_t - \mathrm{bo})}{\mathrm{ao}} = \mathrm{ANN}\left(\frac{(x_t - \mathrm{bi})}{\mathrm{ai}}\right) \quad (3)$$

Where: x_t and y_t are the input and output variables, respectively; ao and bo are the parameters of scale and position of the model outputs; ai and bi are the parameters of scale and position of the model inputs; ANN is the Artificial Neural Network.

The choice of a three-layer architecture was based on the Kolmogorov mapping neural network existence theorem (Hecht-Nielsen, 1987), which stated that any continuous function with n inputs can be implemented exactly by a three-layer feedforward neural network with $2n + 1$ processing elements in the intermediate layer.

The ANN is the model core and is represented by Eq. (4):

$$y = f_o\left(\sum_h w_o f_h\left(\sum_i w_h x + b_h\right) + b_o\right) + e_o \quad (4)$$

Where: x and y are the matrices with inputs (i) and outputs (o), respectively; w_h, b_h, w_o and b_o are the synaptic weight and the tendencies of the hidden layer (h) and the output layer (o), respectively; f_h and f_o are the activation functions, respectively of the hidden and output layers; e_o is the expected error at the output layer.

The activation function used, both for the hidden layer and for the external layer was the unpolar sigmoid, with outputs at the interval [0,1], whose derivate can be calculated

HESSD
12, 3787–3846, 2015

only as a function of the output, and they are represented by Eqs. 5 and 6.

$$a = f(n) = \frac{1}{1 + e^{-n}} \quad (5)$$

$$f'_{(n)} = a(1 - a) \quad (6)$$

Where: a is the output of the activation function; n is the input value.

The network training was performed through the backpropagation algorithm with crossed validation. This algorithm was proposed by Rumelhart et al. (1986), and consists of a method of searching for the synaptic weights to minimize errors, using the so called Delta Rule (Widrow and Hoff, 1960), Eq. (7), which was formulated initially for one-layer neural networks.

$$W_{k+1} = W_k + (\tau e_k \delta_k \mathrm{P}_k) \quad (7)$$

Where: W_k are the current synaptic weights; τ is the learning rate; e_k are the errors of outputs from the layers; δ_k is the derivate of the activation functions; and P_k are the inputs into the layer itself, in iteration k.

In order to apply this method to neural networks with more layers, Eq. (8) is used to estimate the errors in the hidden layers (h), which depend only on the errors and properties of the subsequent layers (s):

$$e_\mathrm{h} = \sum (W_\mathrm{s} e_\mathrm{s} \delta_\mathrm{s}) \quad (8)$$

Where: e_h is the error in the hidden layer; W_s are the synaptic weights in the subsequent layer; e_s are the errors in the subsequent layer, and δ_s are the derivates of the activation function in the subsequent layer.

The ANN hydrological model used was performed in the study of Oliveira et al. (2014), and resulted of the application of an algorithm for simplification of the neural network (Oliveira et al., 2015b). The reduction of input variables and neurons

HESSD
12, 3787–3846, 2015

in the internal layer was performed using an algorithm that looks at the model performance after the imposition of small disturbances in the ANN input data.

The initial ANN model was composed of ten input variables, which included precipitation and evapotranspiration values at times t and $t-1$, mean values of precipitation and evapotranspiration in the previous two months, water balance (difference between precipitation and evapotranspiration) and transformed values by applying an exponential decay filter. After the simplification process it was selected a monthly model for the study area, which presents only three input variables, with four neurons in the hidden layer, totalizing 16 synaptic weights. The inputs are: (i) mean water balance at times t and $t-1$; (ii) weighted mean of the past values of precipitation by applying an exponential decay filter (Hunter, 1986), according to Eq. (9); (iii) weighted mean of the past values of the water balance by applying an exponential decay filter (Eq. 10).

$$fP_t = (1-\alpha) \times fP_{t-1} + \alpha \times P_t. \quad (9)$$

Where: fP_t and fP_{t-1} are the values transformed by applying the exponential decay filter to precipitation, at times t and $t-1$, respectively; P_t is precipitation in time t; α is a coefficient that was calibrated by trials, in order to increase the linear correlation (r) between the filtered variable and the observed flow. In the series used in this study a value equal to 0.52 was obtained for this coefficient.

$$fS_t = (1-\beta) \times fS_{t-1} + \beta \times S_t. \quad (10)$$

Where: fS_t and fS_{t-1} are the values transformed by applying the exponential decay filter to the water balance at times t and $t-1$, respectively; S_t is the water balance at time t; β is a coefficient that was calibrated, similarly to Eq. (9). In the series used in this study, a value equal to 0.41 was obtained for this coefficient.

2.7 Stochastic modeling of monthly flows

According to Salas et al. (1980), if a variable cannot be predicted with certainty, it can be considered a random variable, ruled by the laws of probability. A model can

HESSD
12, 3787–3846, 2015

be defined as stochastic when at least one of the variables involved presents random behavior. According to Salas et al. (1980) the climatic and hydrological variables can be considered random and thus modeled stochastically. In the scientific literature there are numerous references involving the development of stochastic models to generate synthetic climatic and hydrological series (Gabriel and Neumann, 1962; Thomas and Fiering, 1962; Bailey, 1964; Richardson, 1981; Semenov and Barrow, 1997).

In this study a multiplicative type stochastic model was developed to generate monthly flow series. A preliminary analysis of monthly hydrological series was performed to examine the stationarity, seasonality and the temporal dependence. Based on this analysis, for this model, it was adopted the assumption that flow may be estimated by the result of the product of four components that must be estimated in the following sequence: (i) component of long period tendency (C1), that depends on the position in time, month (m) and year (y); (ii) cyclic or seasonal component (C2), that depends only on the month (m); (iii) time dependence component (C3); (iv) random component (C4). In this model the first three components are modeled deterministically, while the random component (C4), being ruled by probability laws, depends only of the adjustment to any probability distribution function.

The product of the four components (Eq. 11), during all the time intervals of modeling, results in a stochastic sequence of monthly flows ($Q_{m/y}$).

$$Q_{m/y} = \mathrm{C1}_{m/y} \times \mathrm{C2}_{m} \times \mathrm{C3} \times \mathrm{C4} \quad (11)$$

In this way, initially, the stochastic modeling process to generate monthly flow series comprised an analysis to look at the stationarity of the observed or simulated series and isolate the tendencies of a long period (C1) This process is necessary to be able to isolate the other components (C2 to C4), both in the base period (1961–1990) and in the future period (2011–2040).

In order to isolate and remove the tendency observed in the series of monthly mean flows during the base period (1961–1990) a linear tendency function was adjusted, represented by Eq. (12), that calculates flow based only on the time interval (axis x, in

HESSD
12, 3787–3846, 2015

months, ranging from 1 to 360). Next, the flow calculated by the linear function (Qtend) is divided by the observed long period mean flow (LPMF), to obtain a correction factor that represents the first component of the model, with a long period tendency (C1), according to Eq. (13). Finally, to obtain a stationary flow (Qst), Eq. (14) was applied, in which the observed flow (Qobs) is divided by component C1.

$$\text{Qtend} = 0.2459x + 98.633 \tag{12}$$

$$\text{C1} = \frac{Q\text{tend}}{\text{LPMF}} \tag{13}$$

$$Q\text{st} = \frac{Q\text{obs}}{C1} \tag{14}$$

In the series of mean monthly flows simulated during the future period (2011–2040) a linear tendency function was also adjusted, represented by Eq. (15) which calculates flow based only on the time interval (x axis, in months, ranging from 1 to 360), to remove the tendency found. Then Eqs. 13 and 14 were applied to obtain the stationary series of monthly flows in the future period (2011–2040).

$$Q\text{tend} = 0.3105x + 143.38 \tag{15}$$

After defining the long period tendency (C1) for both series (base and future), the other components of the model were estimated based on the stationary series. The cyclic or seasonal component ($C2_m$) was calculated as the mean of flows in each month (Table 1), in the base (1961–1990) and future periods (2011–2040).

Then the time dependency component was modeled (C3), which represents the influence of the stream values of the p months before the flow that occurs in the current time. At this stage, the correlation of flow in the current time (t) was analyzed in relation to the previous (t-1, t-2, . . . , t-12), for each month, in the two stationary series (base and future) in which one can find, in general, a significant time dependency up to time t-3, characterizing a model of the third order.

HESSD
12, 3787–3846, 2015

In the multiplicative model, component C3 is a non-dimensional factor, with a mean equal to 1 along the hydrological series, obtained by the ratio between observed flow (stationary), in month m, year y, and mean flow in month m ($C2_m$), as shown by Eq. (16). This equation can only be used when one has observed data. In the case of stochastic modeling, it is assumed that this non-dimensional factor depends only on the value of C3 in the p previous months, thus allowing modeling component C3 at some time interval. The behavior of this component can be modeled by a multiple regression (Eq. 17) or even by a more complex structure, like an ANN with three input variables (Eq. 18).

$$C3 = \frac{Qst_{m/y}}{C2_m} \tag{16}$$

$$C3_t = f(C3_{t-1}, C3_{t-2}, C3_{t-3}) \tag{17}$$

$$C3_t = \mathrm{RNA}(C3_{t-1}, C3_{t-2}, C3_{t-3}) \tag{18}$$

In this study it was chosen to use a model based on ANNs applying the same algorithm detailed in the hydrological modeling stage (Eqs. from 3 to 8), but using as input variables the values of C3 at times $t-1$, $t-2$ and $t-3$, and as expected output the value of C3 at time t. After a few tests and analyses of the results, a neural network was chosen with three neurons in the hidden layer, totalizing 12 synaptic weights.

The random component (C4) is defined as the part that is not explained by the three other deterministic components, i.e., that represents the changes in hydrological behavior provoked by extreme events that occurred in the month. This part of the monthly flow is represented by the ratio between stationary flow (month, m, year y) and the product of the components C2 (month m) and C3, as shown by Eq. (19). As in component C3, the values of C4 tend to a mean value close to 1.

$$C4 = \frac{Qest_{m/y}}{C2_m \times C3} \tag{19}$$

HESSD
12, 3787–3846, 2015

Next, aiming at the generation of synthetic series, first of all it was checked whether component C4 presented any pattern related to the deterministic portion of the model. Considering the stationary series of the base period (1961–1990), it was found that the value of C4 presented two slightly distinct patterns: (i) when the value of C3 is greater than 1, resulting in flow values higher than the monthly mean in the deterministic parcel of the model (high flow periods), the tendency of the random component C4 is to present less dispersed values, varying from 0.33 to 2.83, with a slightly lower mean (0.97); (ii) when the value of C3 is lower than 1, resulting in flows lower than the monthly mean in the deterministic portion of the model (low flow periods), the tendency of C4 is to present greater dispersion, varying from 0.21 to 7.24, with a slightly higher mean (1.03).

The most marked oscillations (inflections or impulses) in the monthly hydrogram which depend on the random component C4, occur predominantly in dry periods, when the flow is below the mean observed for the month. This pattern observed in the historical series explains the smooth tendency found in the values of this component.

Also, considering the stationary series of the future period (2011–2040), when the value of C3 was higher than 1 (high flow periods), the random component C4 presented less dispersed values, ranging from 0.24 to 2.46, with a slightly lower mean (0.99). On the other hand, when the value of C3 was less than 1 (dry periods), component C4 oscillated between 0.13 and 4.98, with a mean of 1.06.

Once the probability curves observed in both periods (base and future) had been observed, a few statistical distributions were adjusted (Gamma, Log-Normal, Weibull, among others) to the values of the random component C4. After the Kolmogorov–Smirnov adherence test was performed, it was found that the Gamma probabilities distribution with three parameters presented the best adjustment to the component modeled. The Gamma distribution with three parameters (ϑ, η, β) is represented by the function given by Eq. (20).

$$f_X(x) = \frac{\zeta^{\eta-1} e^{-\zeta}}{\vartheta \Gamma(\eta)}, \text{com}\, \zeta = \frac{x-\beta}{\vartheta}, \text{para}\, x, \vartheta e \eta > 0 \quad (20)$$

HESSD
12, 3787–3846, 2015

Where: ϑ is a parameter of scale, with the dimension x; β is is a parameter of position, where $\beta < x < \infty$, representing the smallest value of x; η is a shape parameter; $\Gamma(\eta)$ is the Gamma function, normally solved by numerical integration.

After the adjustment of the four components, the stochastic series for both periods were generated, referenced to the parameters calculated based on the two monthly flow series (observed between 1961 and 1990, and simulated between 2011 and 2040). One thousand series with an equal probability of occurrence were generated for each period.

The stochastic modeling process was evaluated comparing the series generated and the series simulated in the future period, from the following aspects: (i) mean monthly flows; (ii) long period mean flow and volume discharged; (iii) SD of monthly flows; (iv) permanence curves.

The changes and uncertainties in water behavior were evaluated by comparing the stochastic series generated for the future period (2011–2040) and the series generated for the base period (1961–1990), considering central values and limits of confidence, looking at the following aspects: (i) mean monthly flows; (ii) SD of monthly flows; (iii) long period mean flow and volume discharged; (iv) permanence curves.

3 Results and discussions

This item will present the results and the discussions held concerning the analysis of stochastic modeling of monthly flows and the changes and uncertainties in water availability in the future period, between 2011 and 2040.

3.1 Analysis of stochastic modeling of monthly flows

The stochastic series generated preserved several characteristics of the original series, simulated for the period between 2011 and 2040. Considering the mean of the 1000 series generated for the future period, the long period mean flow (LPMF) was

HESSD
12, 3787–3846, 2015

200.3 $m^3 s^{-1}$, only 1.1 $m^3 s^{-1}$ (0.5 %) more than the simulated LPMF (original series). This result was also reflected in the accumulated curve of volume discharged (Fig. 3), where the mean difference between the simulated curve (original series) and the central tendency of the 1000 curves generated (stochastic series) was only 4.8 %. Furthermore it can be seen that the smooth tendency of a long period was also preserved, and the values grew more markedly in the final half of the period.

Another characteristic maintained from the original series was the mean monthly flow. Considering the mean of the 1000 series generated for the period between 2011 and 2040 the mean absolute difference was only 0.52 % (Table 2). The greatest absolute difference between mean flows occurred in October, with an overestimation of 1.65 $m^3 s^{-1}$.

Table 2 also shows that the monthly SD was reasonably preserved, with a mean percentage absolute difference of 13.9 % between the original series and the central tendency of the 1000 series generated. The smallest difference was found in the month of October, of only 4.12 $m^3 s^{-1}$ (2.2 %). The greatest difference as to the monthly SD was found in the month of May (43.2 $m^3 s^{-1}$), equivalent to 25.7 %.

Figure 4 illustrates the permanence curves of the mean monthly flow in the future period (2011–2040), in which the similarity between the original series and the central tendency observed in the stochastic series generated becomes clear. The greatest differences were observed in the extremely high flows, with a permanence of less than 2 %. In the rest of the permanence intervals the original curve was always located at the 90 % confidence interval defined by the red lines on the graph.

3.2 Analysis of changes and uncertainties in water availability

The first aspect analyzed as to changes and uncertainties regarding water availability in the future refers to the long period mean flow (LPMF) and to the volume discharged over the period of 30 years. On average, considering the stochastic series in the base period (1961–1990) the LPMF was 141.6 $m^3 s^{-1}$. The confidence interval of LPMF

HESSD
12, 3787–3846, 2015

in the period, with a significance level of 0.1, was between 123.7 and 162.3 $m^3 s^{-1}$ (range 38.6 $m^3 s^{-1}$). On the other hand, in the future period (2011–2040), the projected LPMF was 200.3 $m^3 s^{-1}$, considering the mean value found in the series. This value represents a mean increase of 41.4 % in the LPMF. The confidence interval of LPMF in the future, considering the same level of significance, will be between 165.1 and 233.6 $m^3 s^{-1}$. Thus, the range of the interval will increase from 38.6 to 68.6 $m^3 s^{-1}$.

The change of LPMF according to the projection for the future is also reflected by the mean of the total volume discharged over a 30 year period. Between the years of 1961 and 1990 the mean of the total volume discharged was 132 566 Hm^3. On the other hand, in the future period (2011–2040) the same volume was surpassed on average in 22 years and 10 months. The mean total volume discharged between 2011 and 2040 was 185 869 Hm^3 (Fig. 5).

Considering the stochastic series in the future period, at a 0.1 level of significance, the total volume discharged at the end of 30 years is at the interval between 154 014 Hm^3 and 218 002 Hm^3. This interval is broader and presents values much superior to those observed in the base period, whose total volume varied between 115 462 Hm^3 and 151 454 Hm^3 for the same limit of confidence (Fig. 5).

The second aspect analyzed refers to mean monthly flows. Fig. 6 presents the mean and the 90 % confidence interval for the mean monthly flows, considering the 1000 stochastic series generated during the base and future periods.

The mean monthly flow will increase between the months of January and October, during the period between 2011 and 2040, compared to the base period (1961–1990), with percentages that vary from 14.7 (August) to 118.2 % (March). Besides the month of March, at least four other months will present a significant increase of mean flow: (i) February (113.3 %); (ii) May (110 %); (iii) April (100.7 %); (iv) June (74.1 %). Considering a simple difference between the values obtained in the two periods, the months of May and June presented the greatest changes, with an increased mean monthly flow of 130.5 and 117.7 $m^3 s^{-1}$, respectively. The reduction in mean monthly flow with

HESSD
12, 3787–3846, 2015

percentages of 24.3 and 21 %, respectively, will only occur in the months of November and December.

Considering a statistical analysis of the 1000 stochastic series generated for the two periods analyzed (base and future), at a 0.1 level of significance the confidence interval can be estimated which comprises the mean flow of each month (Fig. 6). The greater the range of this interval, the greater also the uncertainty related to the mean monthly flow.

The range of the 90 % confidence interval for the mean monthly flows will only be reduced in the months of November and December, thus following the tendency observed in the mean monthly values. In November, for instance, the mean flow in the base period, considering the series generated, was between 134.2 and 209.7 $m^3 s^{-1}$ (range of 75.5 $m^3 s^{-1}$). On the other hand, in the future period, the mean flow of the month of November is placed in the interval between 97.2 and 160.7 $m^3 s^{-1}$ (range of 63.6 $m^3 s^{-1}$), a reduction of 11.9 $m^3 s^{-1}$ in the interval (15.8 %). In December, the range of the 90 % confidence interval for mean flow was reduced by 13.5 %, considering the two periods.

In all other months, the range of the confidence interval increased in the future, particularly between the months of February and June, with a greater percentage than 100 %, indicating greater variability between the stochastic series generated and, consequently, greater uncertainties in estimating mean flow. The month of May presented the greatest change in this sense. The mean flow during the base period, considering a 90 % confidence interval was between 95.3 and 144.9 $m^3 s^{-1}$ (range of 49.6 $m^3 s^{-1}$). On the other hand, in the future period, the mean flow in May is inserted into the interval between 187.4 and 314 $m^3 s^{-1}$ (range of 126.6 $m^3 s^{-1}$), a 76.9 $m^3 s^{-1}$ increase in the interval (+155 %).

All the results of mean monthly flows presented indicate a significant change in the hydrological behavior of the Ijuí river basin, considering the climatic projection of the Eta model, between the months of February and June. Between the months of February and June, the confidence intervals do not present any overlap, i.e., the upper limit of

HESSD
12, 3787–3846, 2015

the interval found in the base period is smaller than the lower limit of the interval found in the future.

The third aspect analyzed in the hydrological comparison between the base (1961–1990) and future period (2011–2040) was the SD of mean monthly flows (Table 3). As in the case of the average of the flows in each month, considering the central tendency of the 1000 series generated in the two periods, the SD should increase between the months of January and October, indicating a significant increase in the dispersion of flow values in these months.

The period of the year between the months of February and July is that one where the greatest change occurs in the dispersion of the flow values. In May, for instance, the SD is changed from 82.9 (1961–1990) to 211.2 $m^3 s^{-1}$ (2011–2040), which is a 154.8 % increase for the future (Table 3). On the other hand, the month of November presents a smooth tendency to reduction in the flows with a 121 reduction to 104.2 $m^3 s^{-1}$ (−13.9 %).

When dividing the monthly SD by the mean monthly flow, the coefficients of variation (CV) were obtained for both series, for each month. It can be seen that during the base period (1961–1990), the CV oscillated between 0.698 (February) and 0.716 (November), while in the future period (2011–2040), the same index varied between 0.801 (April) and 0.848 (May). These results indicate a real increase of the monthly variability of flows, with greater fluctuations of monthly flows in the future.

Another aspect analyzed as to changes in hydrological behavior in the future refers to permanence curves of mean monthly flows. Figures 7 and 8 respectively illustrate the mean value and confidence interval of 90 % for the permanence curves of monthly flow, considering the 1000 stochastic series generated in the base (1961–1990) and future periods (2011–2040).

Flows with probability of exceedance equal to or over than 90 % (Q90, Q95, Q99) are important in hydrology for sizing public water supply projects, since they indicates the volume of water that can be guaranteed with the corresponding proportion. As for the flows with probability of exceedance of the order of 50 % (Q50), they are important

HESSD
12, 3787–3846, 2015

to estimate the maximum possible flow to be regularized. Flow rates with probability of exceedance equal to or less than 10 % (Q10, Q5) are used in studies related to extreme flood events.

The flow will be reduced in the future period only at permanence intervals greater than 91 %, i.e., in the portion of lower flows which characterize dry periods. For flows with a permanence equal to or less than Q90 (intermediate and high flow), the tendency is toward increase in the flow values (Fig. 7). As to the range of the 90 % confidence interval for the permanence curve of monthly flows (Fig. 8), the tendency is to increase in the future period, even the lower flows portion. This result illustrates an increase in the uncertainties associated with the estimate of the permanence curve in the future.

On average, considering all the series generated during the base (1961–1990) and future periods (2011–2040), flow with a probability of exceedance equal to or less than 99 % of the months (Q99) was 17.8 and 15 $m^3 s^{-1}$, respectively. This indicates a mean reduction of 15.8 % in Q99 for the future period. Considering a statistical analysis of the stochastic series, at a 0.1 level of significance, we can say that Q99, during the period between 1961 and 1990, is located at the interval between 13.7 and 22.3 $m^3 s^{-1}$, with a range of 8.6 $m^3 s^{-1}$. On the other hand in the future period (2011–2040) this interval changes to values between 10.4 and 20.4 $m^3 s^{-1}$, with a range of 9.9 $m^3 s^{-1}$.

On average, considering all the series generated during the base (1961–1990) and future periods (2011–2040), flow with a probability of exceedance equal to or less than 95 % of the months (Q95) was 30 and 28.5 $m^3 s^{-1}$, respectively. This indicates a mean reduction of 1.5 $m^3 s^{-1}$ (−5.1 %) in Q95 for the future period. This percentage is lower than that observed in Q99, illustrating the tendency to inversion in the permanence curves for larger flows. As for the confidence interval of 90 % of Q95, during the period between 1961 and 1990, the range was 10.4 $m^3 s^{-1}$, with flows between 25 and 35.4 $m^3 s^{-1}$. On the other hand in the future period (2011–2040) this interval lies between 22.4 and 35.8 $m^3 s^{-1}$, with a range of 13.4 $m^3 s^{-1}$.

In the base and future periods, the mean flow with a probability of exceedance equal to or less than 90 % of the months (Q90) was 39.6 and 40.5 $m^3 s^{-1}$, respectively. This

HESSD
12, 3787–3846, 2015

shows a mean increase of 0.9 $m^3 s^{-1}$ (2.2 %) in Q90 for the future period. As to the confidence interval of 90 % of Q90 in the period between 1961 and 1990, the range was 12.4 $m^3 s^{-1}$, with flows between 33.8 and 46.2 $m^3 s^{-1}$. On the other hand in the future period (2011–2040) this interval is between 32.4 and 50.8 $m^3 s^{-1}$, with a range of 18.4 $m^3 s^{-1}$.

In the base period (1961–1990), on average, the flow with a probability of exceedance equal to or less than 50 % of the months (Q50) was 108.2 $m^3 s^{-1}$. At a 0.1 significance level, it can be said that Q50 in this period is inserted into the interval between 94.6 and 122.9 $m^3 s^{-1}$, with a range of 28.2 $m^3 s^{-1}$. On the other hand in the future period, on average, the Q50 was much higher, with a values of 145.1 $m^3 s^{-1}$, indicating a mean increase of 34.2 % for the future. As to the confidence interval, it can be said that the Q50, between 2011 and 2040, will be between 115.8 and 178.1 $m^3 s^{-1}$ (range of 62.3 $m^3 s^{-1}$). Thus, the differences between the confidence intervals of Q50 in the two periods indicate a significant increase in the uncertainties associated with the permanence of flows in future. These results also illustrate a tendency to an increase in the differences between the flows of the base period and the future period inversely proportional to permanence.

In the portion of flows with permanence between 5 (Q5) and 30 % (Q30), the confidence intervals (0.1 significance) of the two periods do not overlap, i.e., the upper limit of the interval during the base period is smaller than the lower limit of the interval in a future period. In the other portions of flows, even if significant differences have been found between the confidence intervals estimated in the base and future periods, they present an overlapping area.

Finally, the changes in the permanence curves of the mean monthly flows in the future, individually, for each month were analyzed. Comparing the permanence curves in the two periods – base (1961–1990) and future (2011–2040) – it can be seen that the smallest changes observed occurred between August and January. In December the absolute mean difference between the permanence curves was 26.1 $m^3 s^{-1}$, and this is the lowest value observed. On the other hand, in May more drastic changes were

HESSD
12, 3787–3846, 2015

observed, with a mean absolute difference of 130.5 $m^3 s^{-1}$ between the permanence curves. Other months that call attention due to the great change in the permanence curves for the future are June (117.7), April (99.5), February (94.1), March (83.7) and July (79.1 $m^3 s^{-1}$).

Figures 9, 10 and 11 illustrate the mean behavior and the 90 % confidence interval for the permanence curves of the monthly flows from January to December, for both periods (base and future). In general, it can be said, based on the results obtained, that between the months of January and October there is tendency for the value of the flows with low permanence to increase – the high flow portion. Regarding this aspect, the main outstanding month is May, in which the mean flow with permanence equal to or less than 10 % (Q10) was 240.4 $m^3 s^{-1}$, between 1961 and 1990, for 573 $m^3 s^{-1}$, in the period between 2011 and 2040, which means an increase of 332.6 $m^3 s^{-1}$ (138 %) in Q10 for the future. Next, the other months between February and July are also outstanding, with an increase in the value of Q10 close to or higher than 200 $m^3 s^{-1}$, as shown in Table 4.

Between the months of February and June, also the flows with a high permanence (portion of the lower flows) presented higher values in the future period compared to the base period, indicating a tendency to a more generalized increase in the flows for these months. In this case, in percentage terms, the month of March is outstanding, in which the mean flow with a probability of exceedance equal to or inferior to 90 % (Q90) was 22.8 $m^3 s^{-1}$, between 1961 and 1990, to 34.5 $m^3 s^{-1}$, in the period between 2011 and 2040, representing an increase of 11.7 $m^3 s^{-1}$ (52 %) in Q90 for the future (Table 4).

On the other hand, in the months of January, July, August, September and October, even lower flow values were observed, with high permanence (low flows), indicating that in those months there was a tendency to amplify the extreme values: dry periods and more intense floods in the future period (2011–2040) than those observed in the base period (1961–1990). In January, for instance, the results indicate a mean increase of 47 % in Q10 and an 8 % reduction in Q90 (Table 4).

HESSD
12, 3787–3846, 2015

In the months of November and December, the tendency observed is for a reduction in the flow values in general, both in the high flow portion and in the low flow portion. As shown in Table 4, in November the results indicate a mean reduction of 18 % ($-61.1\,m^3\,s^{-1}$) in Q10 and 48 % ($-26\,m^3\,s^{-1}$) in Q90. On the other hand, in December for the future period, the mean reduction in Q10 and Q90 was 14 % ($-35.1\,m^3\,s^{-1}$) and 46 % ($-18.2\,m^3\,s^{-1}$), respectively.

Tables 5 and 6 show the limits and ranges of the confidence interval of flows during the base and future periods, with a permanence of 10 (Q10) and 90 % (Q90), respectively. In the case of the ranges of the confidence interval, each month, considering the 1000 stochastic series generated in both periods, there is a clear significant increase in the uncertainties related to the estimate of Q10 and Q90 between the months of January and October. The interval will only be reduced in the months of November and December.

In May, for instance, considering a level of significance of 0.1, the Q10 in the period between 2011 and 2040 is between 388.9 and $804\,m^3\,s^{-1}$, while during the period between 1961 and 1990 the limits were 172.2 and $335.8\,m^3\,s^{-1}$. This considerable change in hydrological behavior can be observed also in the other months, especially between February and July, with growth rates greater than 100 % in range of the 90 % confidence interval for Q10.

In general, the uncertainties regarding the hydrological behavior in the future (2011–2040), taking a single climate scenario as reference, were greater than during the base period (1961–1990). This increase was reflected mainly between the months of January and October, as shown by the results of the comparative analysis between the permanence curves and the mean month flows and their confidence intervals.

The primary source of uncertainties is in the original hydrological series itself, used in the stochastic modeling process. By formulating the stochastic model it is expected that the greater the mean monthly flow (seasonal component, C2), the greater also will be the possibility of obtaining extremely high flows, since this component is multiplied

HESSD
12, 3787–3846, 2015

by the random component (C4) and the time dependence on (C3) which, although they have mean volumes close to 1, may possibly present extreme values.

This becomes clear when compared to the mean monthly flow of each month (in the input series to the stochastic model), with the range of the confidence interval for the mean monthly flow obtained after modeling, considering the 1000 stochastic series, both for the base period (1961–1990) and for the future period (2011–2040), as shown in Fig. 12. There is a visible linear tendency to increased uncertainty as the mean monthly flow increases. However, a clear difference is also observed between the two straight lines that characterize the base and future periods. For a same mean monthly flow, the confidence interval range is higher in the future period series.

After a sensitivity analysis in the models based on ANN to determine the C3 component (time dependency) in both periods, it was found that in the future (2011–2040) the flow in time t is more sensitive because of the antecedent flows ($t-1$, $t-2$ and $t-3$). To illustrate this result, Fig. 13 shows the variation of the value of C3(t) because of the value of C3($t-1$), and the variables C3($t-2$) and C3($t-3$) are maintained equal to 1, for both periods.

In the base period, between 1961 and 1990, even when an extremely low flow occurs in the previous month resulting in a value close to 0 for variable C3($t-1$), the calculated value of C3(t) is almost never less than 0.5, i.e., half the mean monthly flow. On the other hand, in the period between 2011 and 2040, due to the time sequence of the series and its characteristics, the value of C3(t) can be less than 0.3, giving rise to a value well below the mean of that month (Fig. 13).

The same pattern was observed for the portion of the extremely high flows. During the period between 1961 and 1990, when there is a high flow in the previous months, resulting in a value of C3($t-1$), for instance, five times higher than the monthly mean, the calculated value of C3(t) does not reach 2.2. In turn, during the future period, the value of C3(t) may be higher than 3.1, giving rise to a flow that is much higher than the monthly mean (Fig. 13).

HESSD
12, 3787–3846, 2015

In this way the component C3 presents greater fluctuations in the series between 2011 and 2040. This result helps explain the greater variability found between the stochastic series of the future period in relation to the base period.

Figures 14 and 15 illustrate the adjustment in the distribution of Gamma probabilities for modeling the random component (C4) in situations of low flow (C3, in time t, less than 1) and high flow (C3, in time t, higher than 1), respectively.

In general, it is possible to observe that the behavior found in the base series (1961–1990) of the random component C4 was maintained in the series of the future period (2011–2040), especially as regards the months in which the value of C3 was less than 1 (Fig. 14), resulting in a flow lower than the monthly mean. In this case, considering the base and future periods, the chance of the value drawn for C4 being greater than 1 was 42 and 43.5 %, respectively.

On the other hand, in the months when the time dependence component (C3) surpassed the value of 1, the difference between the series was slightly higher (Fig. 15). The probability of a value higher than 1 being drawn for component C4 was 38 and 43 %, respectively, for the base and future series.

These results indicate that the sensitivity of the model to the variable of time dependence also contributed to increasing the uncertainties in the future period, between 2011 and 2040. In the original series simulated for the future period, besides the mean and the dispersion of the data being greater than in the base period, provoking more abrupt fluctuations in the flow values, the correlation coefficient between the flows at times t and $t-1$ was quite high (mean 0.66), with values between 0.5 (November) and 0.78 (March). Already in the period between 1961 and 1990, the correlation coefficient values were between 0.26 (June) and 0.75 (February) with a mean equal to 0.54.

Considering the methodology adopted to model flows in future and to generate the stochastic series, it can therefore be said that there is a certain tendency to an increased hydrological variability during the period between 2011–2040, with a greater dispersion of values in relation to the monthly mean. This finding implies greater un-

HESSD
12, 3787–3846, 2015

certainty regarding the availability of water in the future, with the possible occurrence of time series that are very different from each other.

4 Conclusions

This study analyzed the possible changes and uncertainties related to water availability in the future using a stochastic approach, based on the climate change scenario originating in the LOW member of Eta CPTEC/HadCM3 climate model, for the period between 2011 and 2040. The study was applied to the Ijuí river basin, in the south of Brazil. The methodology involved the correction of the climate variables projected for the future, the hydrological simulation to define a series of monthly flows, and stochastic modeling to generate 1000 hydrological series with an equal probability of occurrence.

As to the stochastic model to generate monthly flow series, several characteristics of the original series were preserved, simulated for the period between 2011 and 2040. Outstanding among them are LPMF and the mean monthly flows, both with differences of only 0.5 %. The monthly SD was reasonably preserved, with a mean percentage absolute difference of 13.9 % between the original series and the central tendency of the 1000 series generated. The similarities between the permanence curves of the monthly flows of the original series and the central tendency observed in the stochastic series generated also became clear. Based on all these results it can be concluded that the stochastic model proposed is adequate to generate monthly flow series.

Various results showed a tendency to increased flows in a general context. The LPMF, for instance, presented an alteration from 141.6 (1961–1990) to 200.3 $m^3 s^{-1}$ (2011–2040), which is a mean increase of 41.4 % in LPMF. Comparing the two periods, the difference between the total volume discharged in 30 years was 53 303 Hm^3. It could also be seen that the mean flow and the monthly SD increased between the months of January and October, in the period between 2011 and 2040. Between the months of February and June the percentage increase of the mean monthly flow was greater than 100 %. It was also found that, in the base period (1961–1990), the co-

HESSD
12, 3787–3846, 2015

efficient of variation (CV) oscillated between 0.698 (February) and 0.716 (November), while for the future period (2011–2040), the same index varied from 0.801 (April) to 0.848 (May), indicating a real increment in the monthly variability of flows, with greater fluctuations in future flows.

Based on the comparison of the permanence curves of monthly flow between the base and future periods, it is concluded that the flow presented lower values (−5.1 %) only at permanence intervals greater than 90 % in the dry months. For flows with a permanence equal to or less than Q90 (intermediate and high flow), there is a tendency for the flow values to increase. For instance, in the base period (1961–1990), on average, the flow with permanence equal to or less than 50 % of the months (Q50) was 108.2 $m^3 s^{-1}$. On the other hand, in the future period Q50 was much higher, with a value of 145.1 $m^3 s^{-1}$ (34.2 % increase).

It can also be observed that the smaller changes in flow permanence occurred between the months of August and January. On the other hand, in the other months, the changes were drastic. In May, for instance, an absolute mean difference was found of 130.5 $m^3 s^{-1}$ between the permanence curves.

In general it is concluded, based on the results obtained that between the months of January and October there is tendency for the flood flows to increase. Between the months of February and June, also the flows with high permanence (minimum flows) presented higher values in the future compared to the base period. On the other hand, in the months of January, July, August, September and October, even lower minimum flow values were observed, indicating that in these months there is tendency to amplify the extreme values. Finally, in the months of November and December the tendency observed is for the reduction of flow values, in general, both in the high flow and in the low flow portions.

As to the uncertainties concerning the hydrological behavior and, consequently, water availability for the future, having as reference the results and discussions presented, it is concluded that uncertainties regarding hydrological behavior between 2011 and 2040 were greater than in the base period. The main factor that contributed to this re-

HESSD
12, 3787–3846, 2015

sult was the increase of the mean itself and of the SD of monthly flows. Besides these, in the future, time dependency will present a more marked contribution to the composition of monthly flow, making the model more sensitive to abrupt variation in flow the previous month.

In this way, considering the stochastic series generated for the future, it can be said that there is a certain tendency for the increase hydrological variability during the period between 2011–2040. This finding means greater uncertainty regarding water availability in the future, with the possibility that time series may occur with marked differences as to the occurrence of drought and flood periods.

Acknowledgements. We are grateful to FINEP for funding the research – MCT/FINEP CT-HIDRO 01/2010 – Convênio 01.12.0396.00, Project: Research Network in Monitoring and Modeling Hydrosedimentological Processes in Representative Rural and Urban Basins of the Atlantic Forest Biome (RHIMA). We thank CNPq for the doctoral scholarship of the first author of this study and for the Research Productivity Grant for the third author.

References

Allen, R. G., Pereira, L. S., Raes, K., and Smith, M.: Crop evapotranspiration (guidelines for computing crop water requirements), Irrig. Drain., 56, http://www.fao.org/docrep/X0490E/x0490e00.htm, ISBN 92-5-104219-5, 1998.

Arnell, N. W.: Climate change and global water resources, Global Environ. Chang., 9, 31–49, 1999.

Arnell, N. W.: Climate change and global water resources: SRES emissions and socio-economic scenarios, Global Environ. Chang., 14, 31–52, 2004.

Bailey, N. T. J.: The Elements of Stochastic Processes, Wiley, New York, 1964.

Bárdossy, A. and Pegram, G.: Downscaling precipitation using regional climate models and circulation patterns toward hydrology, Water Resour. Res., 47, W04505, doi:10.1029/2010WR009689, 2011.

Bergström, S., Carlsson, B., Gardelin, M., Lindström, G., Pettersson, A., and Rummukainen, M.: Climate change impacts on runoff in Sweden – assessments by global climate models, dynamical downscaling and hydrological modeling, Climate Res., 16, 101–112, 2001.

HESSD

12, 3787–3846, 2015

Betts, A. K. and Miller, M. T.: A new convective adjustment scheme, Part II: Single column tests using GATE wave, BOMEX, ATEX and arctic air-mass data sets, Q. J. Roy. Meteor. Soc., 112, 693–703, 1986.

Black, T. L.: NMC notes, the new NMC mesoscale Eta Model: description and forecast examples, Weather. Anal. Forecast. , 9, 256–278, 1994.

Boé, J., Terray, L., Habets, F., and Martin, E.: Statistical and dynamical downscaling of the Seine basin climate for hydro-meteorological studies, Int. J. Climatol., 27, 1643–1655, 2007.

Booij, M. J.: Impact of climate change on river flooding assessed with different spatial model resolutions, J. Hydrol., 303, 176–198, 2005.

Bowden, G. J., Dandy, G. C., and Maier, H. R.: Input determination for neural network models in water resources applications, Part I – background and methodology, J. Hydrol., 301, 75–92, 2005.

Castro, N. M. R., Auzet, A. V., Chevallier, P., and Leprun, J. C.: Land use change effects on runoff and erosion from plot to catchment scale on the basaltic plateau of Southern Brazil, Hydrol. Process., 13, 1621–1628, 1999.

Chou, S. C., Marengo, J. A., Lyra, A., Sueiro, G., Pesquero, J., Alves, L. M., Kay, G., Betts, R., Chagas, D., Gomes, J. L. Bustamante, J., and Tavares, P.: Downscaling of South America present climate driven by, 4-member HadCM3 runs, Clim. Dynam., 38, 635–653, doi:10.1007/s00382-011-1002-8, 2012.

Ek, M. B., Mitchell, K. E., Lin, Y., Rogers, E., Grummen, P., Koren, V., Gayno, G., and Tarpley, J. D.: Implementation of NOAH land surface advances in the National Centers for Environmental Prediction operational mesoscale Eta Model, Geophys. Res. , 108, 8851, doi:10.1029/2002JD003246, 2003.

Fels, S. B. and Schwarzkopf, M. D.: The simplified exchange approximation: a new method for radiative transfer calculations, J. Atmos. Sci., 32, 1475–1488, 1975.

Gabriel, R. and Neumann, J.: A Markov Chain Model for daily rainfall occurrence in Tel Aviv, Israel, Q. J. Roy. Meteor. Soc., 88, 90–95, 1962.

Graham, L. P.: Large-scale hydrological modeling in the Baltic basin, Division of Hydraulic Engineering, Dept of Civil and Environmental Engineering, Report TRITA-AMI PHD 1033, Royal Institute of Technology, Stockholm, 2000.

Graham, L. P.: Climate change effects on river flow to the Baltic Sea, Ambio, 33, 235–241, 2004.

HESSD

12, 3787–3846, 2015

Gunawardhana, L. N. and Kazama, S.: A water availability and low-flow analysis of the Tagliamento River discharge in Italy under changing climate conditions, Hydrol. Earth Syst. Sci., 16, 1033–1045, doi:10.5194/hess-16-1033-2012, 2012.
Hecht-Nielsen, R.: Kolmogorov's mapping neural network existence theorem, Proceedings of the First IEEE International Joint Conference on Neural Networks, 21–24 June, San Diego, California, IEEE: New York, 11–14, 1987.
Hughes, D. A., Kingston, D. G., and Todd, M. C.: Uncertainty in water resources availability in the Okavango River basin as a result of climate change, Hydrol. Earth Syst. Sci., 15, 931–941, doi:10.5194/hess-15-931-2011, 2011.
Hunter, J. S.: The exponentially weighted moving average, J. Qual. Technol., 18, 203–210, 1986.
Intergovernmental Panel On Climate Change - IPCC: Climate Change 2013: The physical science basis, working group I contribution to the Fifth Assessment Report of the IPCC, Stockholm, September, 2216p, 2013.
Jain, A. and Kumar, A. M.: Hybrid neural network models for hydrologic time series forecasting, Appl. Soft. Comput., 7, 585–592, 2007.
Janjic, Z. I.: The step-mountain eta coordinate model: further developments of the convection, viscous sublayer and turbulence closure schemes, Mon. Weather Rev., 122, 927–945, 1994.
Kaczmarek, Z., Napiórkowski, J., and Strzepek, K. M.: Climate change impacts on the water supply system in the Warta River Catchment, Poland, Int. J. Water Resour. , 12, 165–180, 1996.
Kleinn, J., Frei, C., Gurtz, J., Lüthi, D., Vidale, P. L., and Schär, C.: Hydrologic simulations in the Rhine basin driven by a regional climate model, J. Geophys. Res., 110, D04102, 2005.
Lacis, A. A. and Hansen, J. E.: A parameterization of the absorption of solar radiation in earth's atmosphere, J. Atmos. Sci., 31, 118–133, 1974.
Leahy, P., Kiely, G., and Corcoran, G.: Structural optimisation and input selection of an artificial neural network for river level prediction, J. Hydrol., 355, 192–201, 2008.
Lenderink, G., Buishand, A., and van Deursen, W.: Estimates of future discharges of the river Rhine using two scenario methodologies: direct versus delta approach, Hydrol. Earth Syst. Sci., 11, 1145–1159, doi:10.5194/hess-11-1145-2007, 2007.
Lettenmaier, D. P., Wood, A. W., Palmer, R. N., Wood, E. F., and Stakhiv, E. Z.: Water resources implications of global warming: A. U. S. regional perspective, Clim. Chang. , 43, 537–579, 1999.

HESSD
12, 3787–3846, 2015

Marengo, J. A., Jones, R., Alves, L. M., and Valverde, M. C.: Future change of temperature and precipitation extremes in South America as derived from the PRECIS regional climate modeling system, Int. J. Climatol., 29, 2241–2255, doi:10.1002/joc.1863, 2009.

Marengo, J. A., Chou, S. C., Kay, G., Alves, L., Pesquero, J. F., Soares, W. R., Santos, D. C., Lyra, A. A., Sueiro, G., Betts, R., Chagas, D. J., Gomes, J. L., Bustamante, J. F., and Tavares, P.: Development of regional future climate change scenarios in South America using the Eta CPTEC/HadCM3 climate change projections: climatology and regional analyses for the Amazon, São Francisco and the Parana River Basins, Clim. Dynam., 38, 1829–1848, 2012.

Maurer, E. P. and Hidalgo, H. G.: Utility of daily vs. monthly large-scale climate data: an intercomparison of two statistical downscaling methods, Hydrol. Earth Syst. Sci., 12, 551–563, doi:10.5194/hess-12-551-2008, 2008.

Mearns, L. O., Rosenzweig, C., and Goldberg, R.: The effect of changes in daily and interannual climatic variability on CERES-wheat yields: a sensitivity study, Clim. Chang. , 32, 257–292, 1996.

Mellor, G. F. and Yamada, T.: A hierarchy of turbulence closure models for boundary layers, J. Atmos. Sci., 31, 1791–1806, 1974.

Menzel, L. and Bürger, G.: Climate change scenarios and runoff response in the Mulde catchment (Southern Elbe, Germany), J. Hydrol., 267, 53–64, 2002.

Middelkoop, H., Daamen, K., Gellens, D., Grabs, W., Kwadijk, J. C. J., Lang, H., Parmet, B. W. A. H., Schädler, B., Schulla, J., and Wilke, K.: Impact of climate change on hydrological regimes and water resources management in the Rhine Basin, Clim. Chang. , 49, 105–128, 2001.

Milly, P. C. D., Dunne, K. A., and Vecchia, A. V.: Global pattern of trends in streamflow and water availability in a changing climate, Nature, 438, 347–350, 2005.

Monteith, J. L.: Evaporation and environment, Symp. Soc. Exp. Biol. , 19, 205–234, 1965.

Nijssen, B., O'Donnell, G. M., Hamlet, A. F., and Lettenmaier, D. P.: Hydrologic sensitivity of global rivers to climate change, Clim. Chang. , 50, 143–175, 2001.

Nohara, D., Kitoh, A., Hosaka, M., and Oki, T.: Impact of climate change on river discharge projected by multimodel ensemble, J. Hydrometeorol., 7, 1076–1089, 2006.

Oliveira, G. G., Pedrollo, O. C., and Castro, N. M. R.: O desempenho das Redes Neurais Artificiais (RNAs) para simulação hidrológica mensal, Revista Brasileira de Recursos Hídricos , 19, 251–265, 2014.

HESSD
12, 3787–3846, 2015

Oliveira, G. G., Pedrollo, O. C., and Castro, N. M. R.: As incertezas associadas às condições climáticas obtidas pelo modelo Eta CPTEC/HadCM3: avaliação comparativa entre os dados simulados e observados de precipitação, evapotranspiração e vazão na bacia hidrográfica do rio Ijuí, Brasil, Revista Brasileira de Meteorologia , 30, 101–121, 2015a.

Oliveira, G. G., Pedrollo, O. C., and Castro, N. M. R.: Simplifying artificial neural network models of river basin behaviour by an automated procedure for input variable selection, Eng. Appl. Artif. Intel., 40, 47–61, 2015b.

Panofsky, H. A. and Brier, G. W.: Some Applications of Statistics to Meteorology, The Pennsylvania State University, University Park, 1968.

Penman, H. L.: Natural evaporation from open water, bare soil and grass, P. R. Soc. London, A193, 120–145, 1948.

Pesquero, J. F.: Balanço de umidade na região do sistema de monção da América do Sul em cenários climáticos futuros (2071–2100) utilizando o modelo Eta: um estudo de modelagem, Tese de Doutoradom, São José dos Campos, INPE, 2009.

Piani, C., Weedon, G. P., Best, M., Gomes, S. M., Viterbo, P., Hagemann, S., and Haerter, J. O.: Statistical bias correction of global simulated daily precipitation and temperature for the application of hydrological models, J. Hydrol., 395, 199–215, doi:10.1016/j.jhydrol.2010.10.024, 2010.

Rasmussen, J., Sonnenborg, T. O., Stisen, S., Seaby, L. P., Christensen, B. S. B., and Hinsby, K.: Climate change effects on irrigation demands and minimum stream discharge: impact of bias-correction method, Hydrol. Earth Syst. Sci., 16, 4675–4691, doi:10.5194/hess-16-4675-2012, 2012.

Richardson, C. W.: Stochastic simulation of daily precipitation, temperature and solar radiation, Water Resour. Res., 17, 182–190, 1981.

Richter, G. M. and Semenov, M. A.: Modelling impacts of climate change on wheat yields in England and Wales: assessing drought risks, Agr. Syst., 84, 77–97, 2005.

Rossato, M. S.: Os climas do Rio Grande do sul: variabilidade, tendências e tipologia, Tese de Doutorado, UFRGS/PPGEA, Porto Alegre, 2011.

Rumelhart, D. E., Hinton, G. E., and Williams, R. J.: Learning representations by back-propagating errors, Nature, 323, 533–536, 1986.

Salas, J. D., Delleur, J. W., Yevjevich, V., and Lane, W. L.: Applied Modeling of Hydrologic Time Series, Water Resources Publications: Littleton, Colorado, USA, 1980.

HESSD
12, 3787–3846, 2015

Semenov, M. A. and Barrow, E. M.: Use of a stochastic weather generator in the development of climate change scenarios, Clim. Chang. , 35, 397–414, 1997.
Sibson, R.: A brief description of natural neighbor interpolation, in: Interpreting Multivariate Data, edited by: Barnett, V., Wiley, Chichester, 21–36, 1981.
Silva, V. S. V., Pedrollo, O. C., Castro, N. M. R., and Lucchese, L. V.: Estudo de regionalização por transferência de parâmetros do Modelo IPH II na bacia do Rio Ijuí/RS, Revista de Gestão de Água da América Latina , 10, 65–75, 2013.
Themeßl, M. J., Gobiet, A., and Leuprecht, A. Empirical-statistical downscaling and error correction of daily precipitation from regional climate models, Int. J. Climatol., 31, 1531–1544, 2011.
Themeßl, M. J., Gobiet, A., and Heinrich, G.: Empirical-statistical downscaling and error correction of regional climate models and its impact on the climate change signal, Clim. Chang. , 112, 449–468, 2012.
Thomas, H. A. and Fiering, M. B.: Mathematical synthesis of streamflow sequences for the analysis of river basins by simulation, in: Design of water resources systems, edited by: Mass, A., Hufschmidt, M. M., Dorfman, R., Thomas, H. A., Marglin, S. A., and Fair, G. M., Harvard University Press, Cambridge, Massachusetts, 459–493, 1962.
Widrow, B. and Hoff, M. E.: Adaptive switching circuits, in: 1960 IRE WESCON Convention Record, IRE Part 4, http://www-isl.stanford.edu/~widrow/papers/c1960adaptiveswitching.pdf, New York, 96–104, 1960.
Wilks, D. S.: Adapting stochastic weather generation algorithms for climate change studies, Clim. Chang. , 22, 67–84, 1992.
Wood, A. W., Leung, L. R., Sridhar, V., and Lettenmaier, D. P.: Hydrologic implications of dynamical and statistical approaches to downscale climate model outputs, Clim. Chang. , 62, 189–216, 2004.
Zhang, X. C. and Liu, W. Z.: Simulating potential response of hydrology, soil erosion, and crop productivity to climate change in Changwu tableland region on the Loess Plateau of China, Agr. Forest Meteorol., 131, 127–142, 2005.
Zhao, Q., Black, T. L., and Baldwin, M. E.: Implementation of the cloud prediction scheme in the Eta Model at NCEP, Weather Forecast., 12, 697–712, 1997.

HESSD
12, 3787–3846, 2015

Table 1. Cyclic (seasonal) component in the base and future periods: mean monthly flow in the Ijuí River basin, Santo Ângelo station.

Month	Mean monthly flow ($m^3 s^{-1}$)	
	Base (1961–1990)	Future (2011–2040)
Jan	99.7	126.4
Feb	85.8	181.1
Mar	74.7	159.7
Apr	95.8	200.5
May	114.9	249.1
Jun	160.0	280.3
Jul	180.8	263.6
Aug	199.0	212.8
Sep	228.5	264.1
Oct	187.2	228.4
Nov	166.7	128.2
Dec	126.3	95.8

HESSD
12, 3787–3846, 2015

Table 2. Difference between the original series (simulated) and the 1000 stochastic series generated – mean flow and monthly SD in the period between 2011 and 2040, Santo Ângelo gauge station.

Month	Mean monthly flow ($m^3 s^{-1}$)			Monthly SD ($m^3 s^{-1}$)		
	Original series	Mean of series generated	Percentage difference	Original series	Mean of series generated	Percentage difference
Jan	128.7	127.6	−0.83 %	118.0	102.5	−13.13 %
Feb	178.5	177.2	−0.74 %	179.3	142.2	−20.67 %
Mar	155.4	154.5	−0.62 %	143.7	124.0	−13.73 %
Apr	199.2	198.2	−0.48 %	163.2	158.8	−2.66 %
May	249.6	249.2	−0.16 %	168.0	211.2	25.70 %
Jun	276.5	276.5	0.01 %	195.0	224.0	14.87 %
Jul	262.5	262.9	0.16 %	183.5	213.4	16.29 %
Aug	217.7	218.3	0.27 %	149.4	175.5	17.44 %
Sep	268.1	269.5	0.52 %	205.2	216.6	5.54 %
Oct	228.9	230.6	0.72 %	183.9	188.0	2.24 %
Nov	126.9	128.0	0.86 %	83.8	104.2	24.43 %
Dec	97.0	97.9	0.93 %	87.8	78.9	−10.11 %

HESSD
12, 3787–3846, 2015

Table 3. Mean of SD of monthly flows during the base and future periods – Santo Ângelo gauge station.

Month	Mean monthly SD ($m^3 s^{-1}$)	
	Base (1961–1990)	Future (2011–2040)
Jan	67.7	102.5
Feb	58.0	142.2
Mar	49.9	124.0
Apr	69.2	158.8
May	82.9	211.2
Jun	112.1	224.0
Jul	131.9	213.4
Aug	134.9	175.5
Sep	161.0	216.6
Oct	131.0	188.0
Nov	121.0	104.2
Dec	88.6	78.9

HESSD
12, 3787–3846, 2015

Table 4. Mean flows ($m^3 s^{-1}$) with 10 % (Q10) and 90 % (Q90) permanence during the base period (1961–1990) and future period (2011–2040) – Santo Ângelo gauge station.

Month	Base (1961–1990)		Future (2011–2040)		Changes	Changes
	Q10	Q90	Q10	Q90	Q10	Q90
Jan	195.2	30.5	286.0	28.1	90.8	−2.4
Feb	168.6	26.8	393.5	39.2	224.9	12.4
Mar	145.3	22.8	343.0	34.5	197.7	11.7
Apr	201.4	31.7	438.1	44.4	236.7	12.7
May	240.4	38.7	573.0	50.2	332.6	11.5
Jun	324.0	51.5	610.5	61.6	286.5	10.1
Jul	376.5	58.9	582.9	58.2	206.4	−0.7
Aug	390.2	61.0	486.4	48.5	96.3	−12.5
Sep	463.6	72.6	594.5	60.9	130.9	−11.7
Oct	376.4	59.4	517.2	50.6	140.8	−8.8
Nov	345.7	54.1	284.6	28.1	−61.1	−26.0
Dec	252.2	39.8	217.1	21.6	−35.1	−18.2

HESSD
12, 3787–3846, 2015

Table 5. Limits and ranges of the confidence interval of flows ($m^3 s^{-1}$) with a permanence of 10 % (Q10) during the base period (1961–1990) and future period (2011–2040), Santo Ângelo gauge station.

Month	Base (1961–1990)			Future (2011–2040)		
	Lower limit	Upper limit	Range	Lower limit	Upper limit	Range
Jan	136.3	275.3	139.0	196.3	395.4	199.0
Feb	117.6	232.6	115.0	272.3	548.0	275.7
Mar	102.5	201.3	98.9	236.7	474.6	238.0
Apr	141.3	285.0	143.8	305.4	620.1	314.7
May	172.2	335.8	163.6	388.9	804.0	415.1
Jun	229.6	451.4	221.8	420.1	855.8	435.7
Jul	261.9	526.2	264.3	403.8	790.2	386.4
Aug	274.1	541.5	267.4	333.8	679.1	345.3
Sep	325.1	648.0	323.0	400.7	828.7	428.0
Oct	269.3	515.8	246.5	352.6	723.1	370.5
Nov	245.4	485.3	239.9	197.1	400.5	203.3
Dec	174.3	352.6	178.3	151.6	297.3	145.7

HESSD
12, 3787–3846, 2015

Table 6. Limits and ranges of the confidence interval of flows ($m^3 s^{-1}$) with 90 % permanence (Q90) in the base period (1961–1990) and future period (2011–2040), Santo Ângelo gauge station.

Month	Base (1961–1990)			Future (2011–2040)		
	Lower limit	Upper limit	Range	Lower limit	Upper limit	Range
Jan	20.4	42.9	22.5	16.6	43.3	26.7
Feb	17.9	38.0	20.1	23.8	60.0	36.2
Mar	15.2	32.0	16.8	20.5	53.6	33.0
Apr	21.5	43.7	22.2	26.1	68.9	42.8
May	25.9	53.3	27.4	29.8	80.1	50.3
Jun	34.6	71.3	36.7	35.7	95.3	59.6
Jul	38.9	83.4	44.4	34.4	87.7	53.3
Aug	41.4	85.3	43.9	28.7	72.9	44.2
Sep	48.9	100.1	51.2	37.0	93.9	56.9
Oct	39.6	82.5	42.8	30.9	77.4	46.6
Nov	35.8	76.3	40.4	16.6	43.6	27.1
Dec	26.5	55.9	29.4	12.9	32.5	19.6

HESSD
12, 3787–3846, 2015

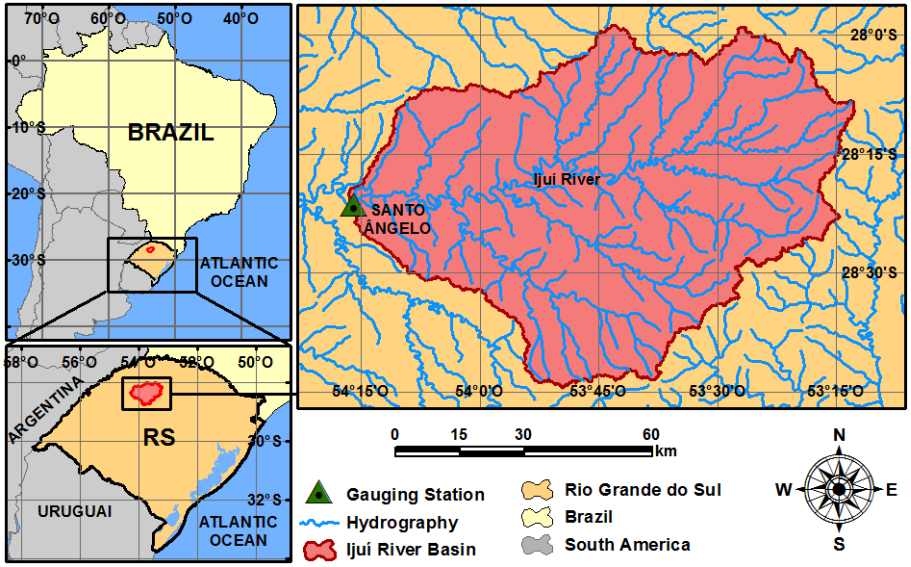

Figure 1. Location of the Ijuí River basin, section upstream from the Santo Ângelo gauging station (5414 km^2), RS, Brazil.

HESSD
12, 3787–3846, 2015

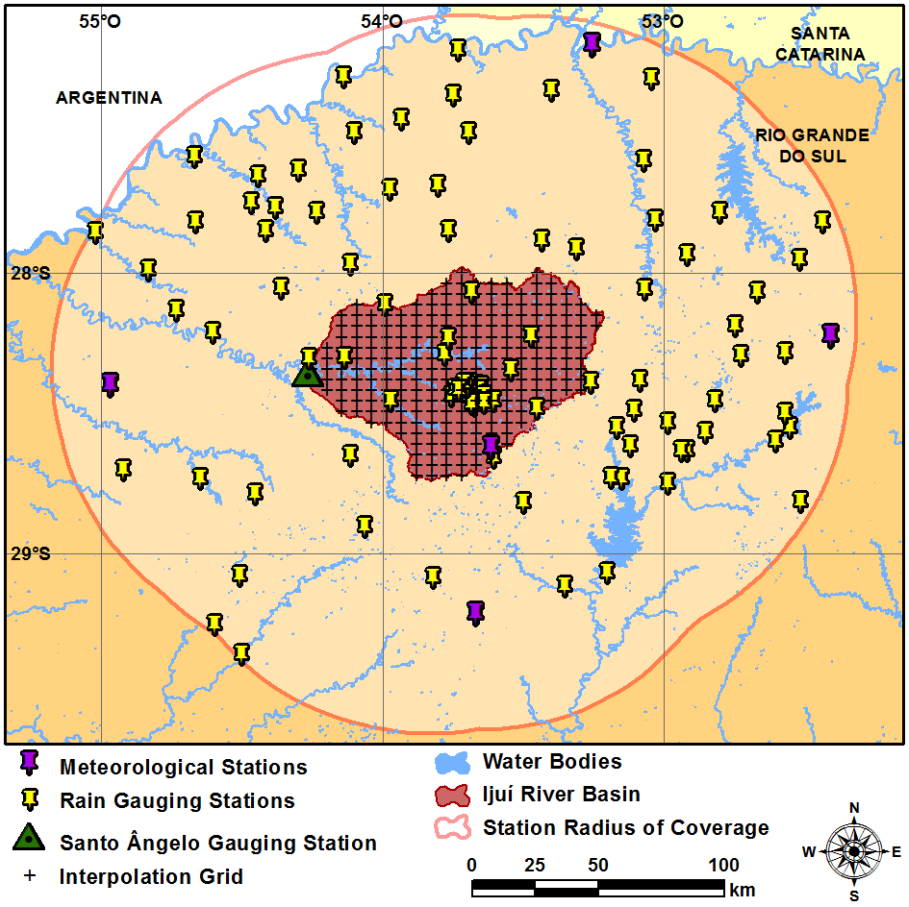

Figure 2. Location of the stations with hydrologic and climate data used in a radius of coverage of 100 km in relation to the Ijuí River basin.

HESSD
12, 3787–3846, 2015

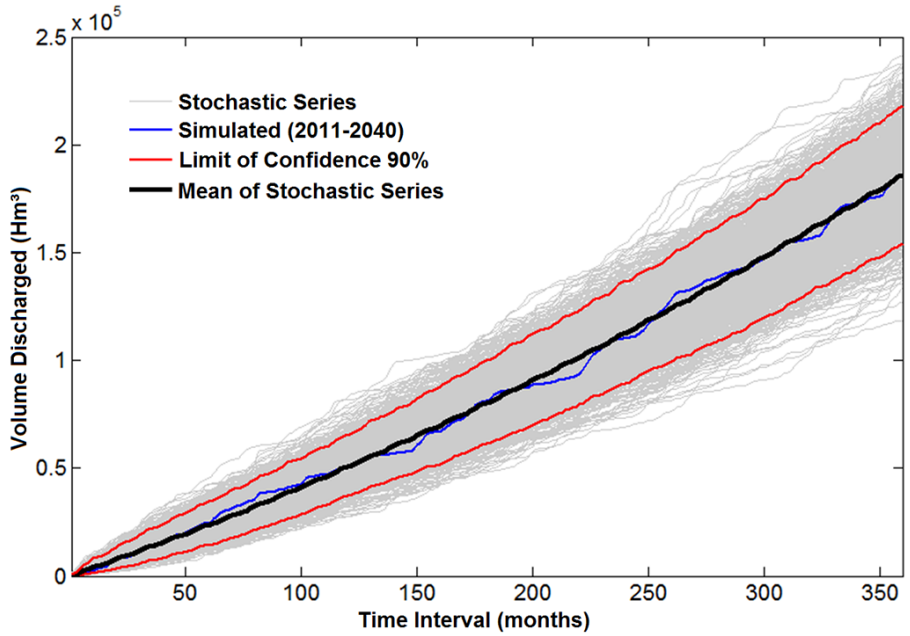

Figure 3. Curves of volume discharged in the future (2011–2040) – difference between the original series (simulated) and the 1000 stochastic series generated – Ijuí River basin, Santo Ângelo gauge station.

HESSD
12, 3787–3846, 2015

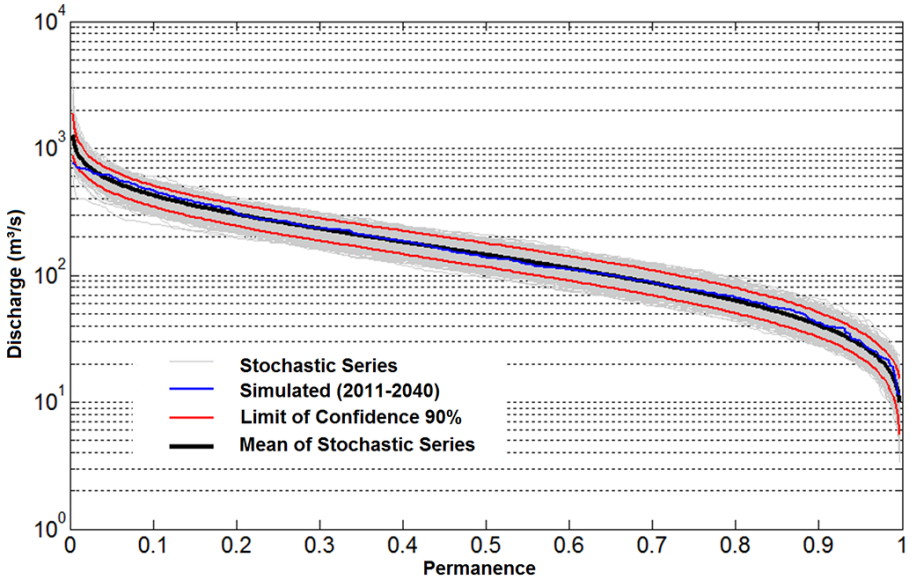

Figure 4. Permanence curves for the mean monthly flow between 2011 and 2040 – difference between the original series (simulated) and the 1000 stochastic series generated – Santo Ângelo gauge station.

HESSD
12, 3787–3846, 2015

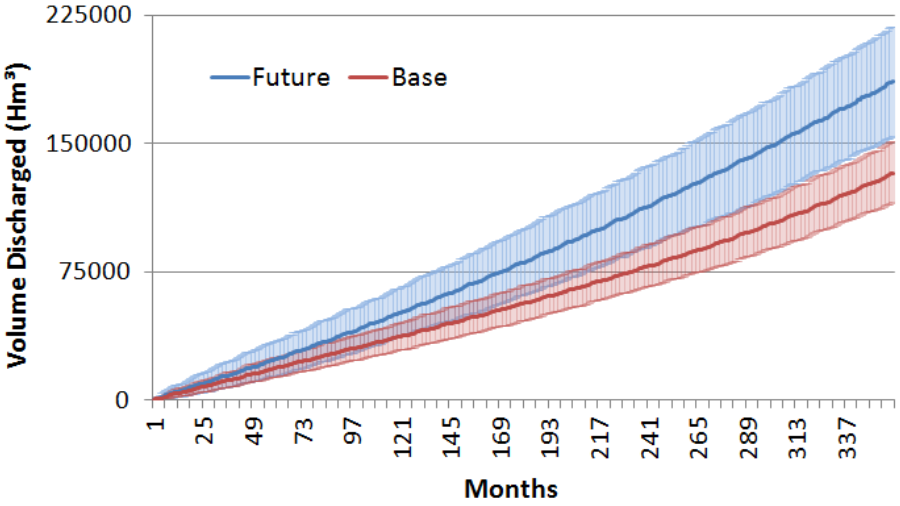

Figure 5. Mean and 90 % confidence interval for the volume discharged, based on the stochastic series generated, base period (1961–1990) and future period (2011–2040), Santo Ângelo gauge station.

HESSD
12, 3787–3846, 2015

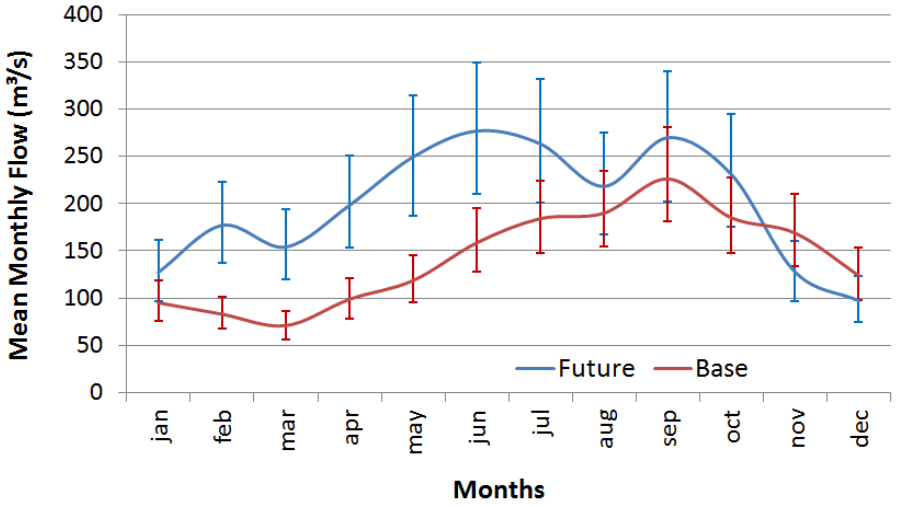

Figure 6. Mean and 90 % confidence interval for the mean monthly flows based on the stochastic series generated, during the base (1961–1990) and future periods (2011–2040), at Santo Ângelo gauge station.

HESSD
12, 3787–3846, 2015

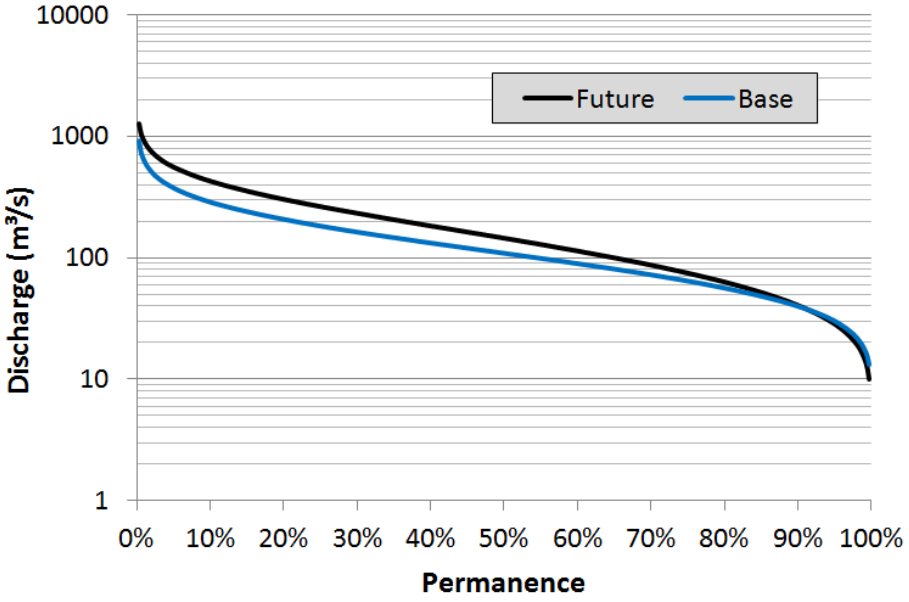

Figure 7. Mean value of permanence curves of monthly flow according to the stochastic series generated during the base (1961–1990) and future periods (2011–2040), at Santo Angelo gauge station.

HESSD
12, 3787–3846, 2015

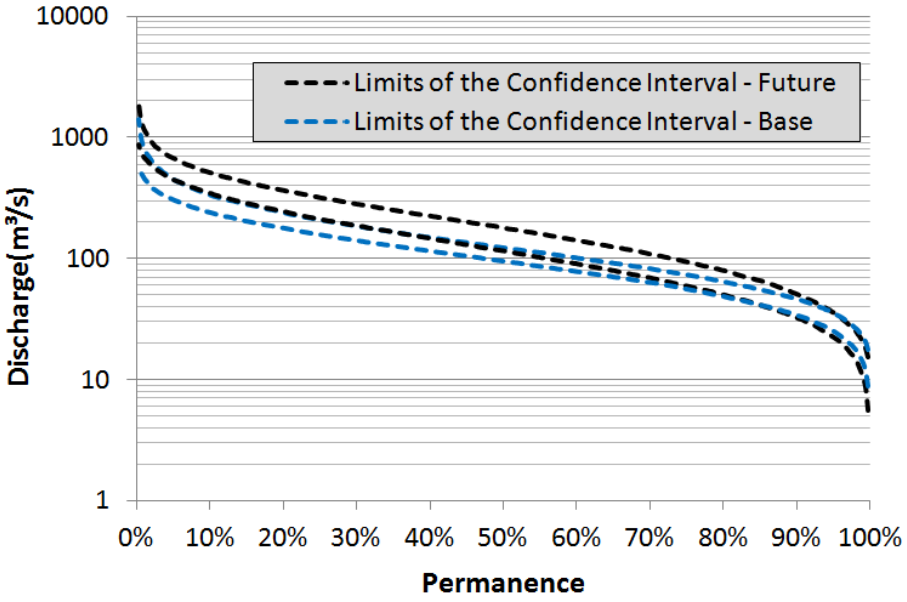

Figure 8. 90 % confidence interval for the monthly flow permanence curves, according to the stochastic series generated in the base (1961–1990) and future periods (2011–2040) – Santo Ângelo gauge station.

HESSD
12, 3787–3846, 2015

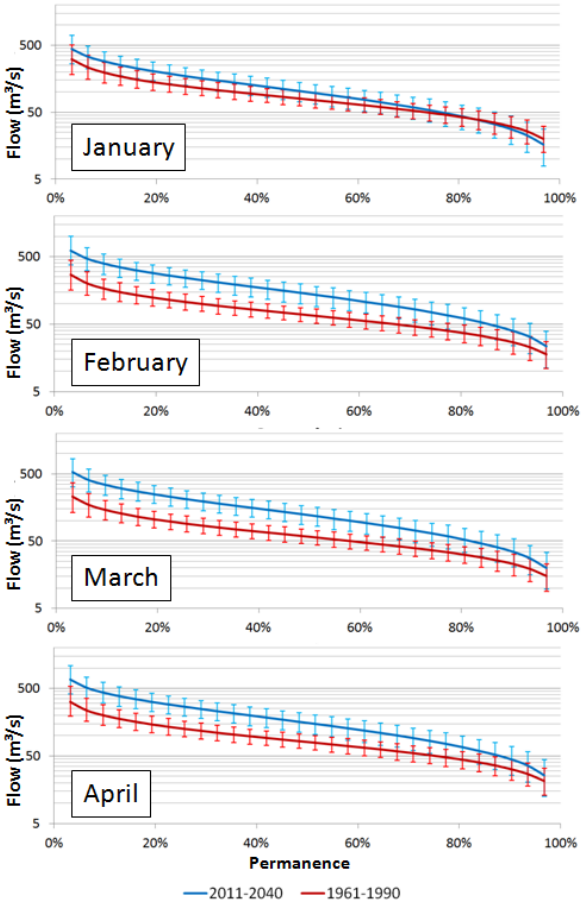

Figure 9. Mean and 90 % confidence interval for the monthly flow permanence curves at Santo Ângelo gauge station, according to the stochastic series generated in the base period (1961–1990) and future period (2011–2040): January, February, March and April.

HESSD
12, 3787–3846, 2015

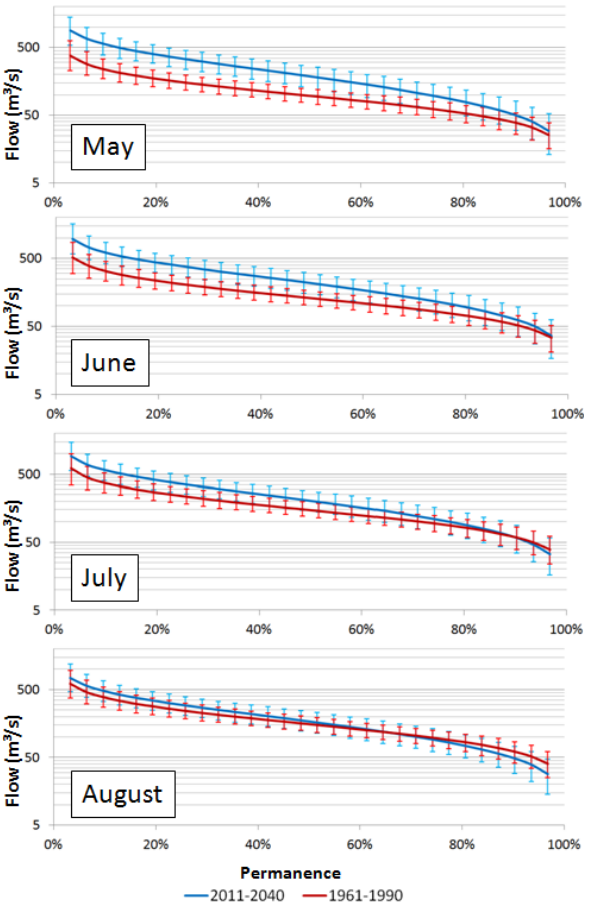

Figure 10. Mean and 90 % confidence interval for the monthly flow permanence curves at Santo Ângelo gauge station, according to the stochastic series generated in the base period (1961–1990) and future period (2011–2040): May, June, July and August.

HESSD
12, 3787–3846, 2015

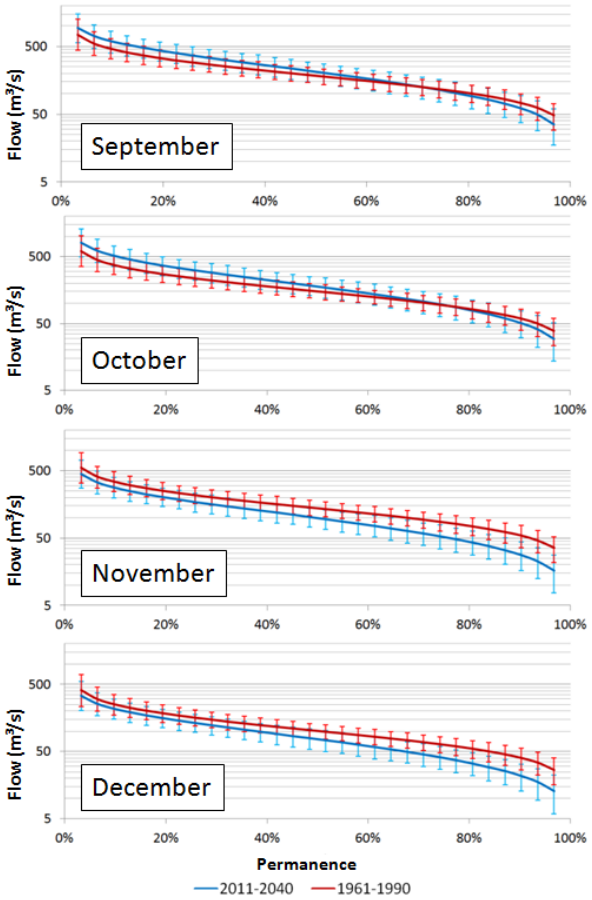

Figure 11. Mean and 90 % confidence interval for the monthly flow permanence curves at Santo Ângelo gauge station, according to the stochastic series generated in the base period (1961–1990) and future period (2011–2040): September, October, November and December.

HESSD
12, 3787–3846, 2015

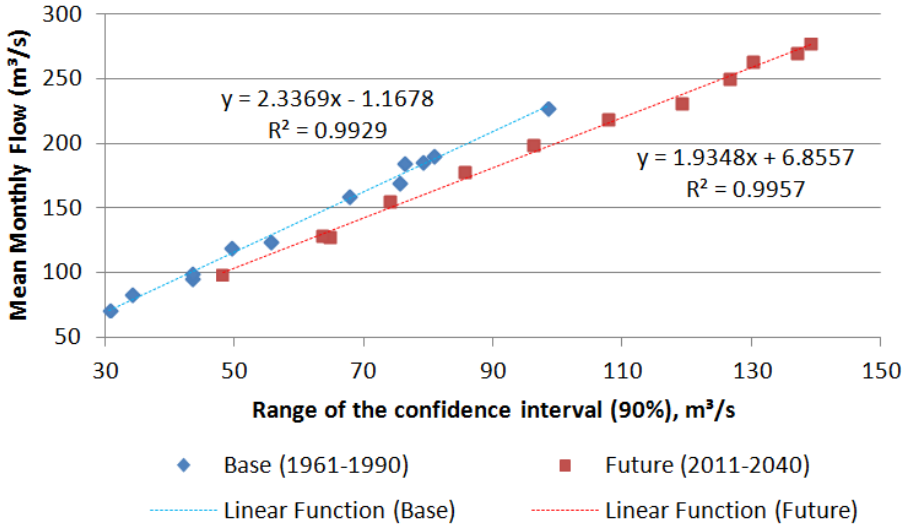

Figure 12. Relationship between the mean of the monthly flow and the range of the confidence interval for the periods between 1961 and 1990 (base) and between 2011 and 2040 (future).

HESSD
12, 3787–3846, 2015

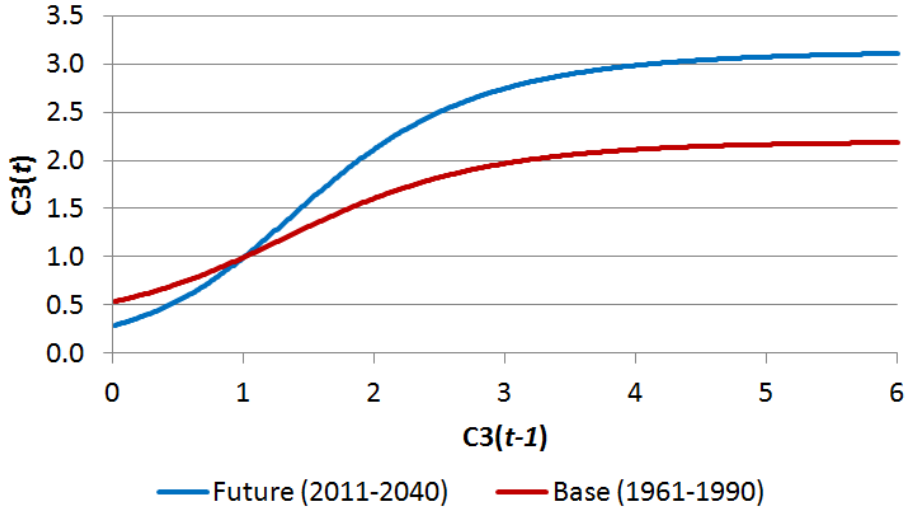

Figure 13. Variation of the value of C3(t), based on the value of C3(t-1), in modeling the time dependence component using ANN, keeping the other variables, C3(t-2) and C3(t-3), equal to 1 for the periods between 1961 and 1990 (base) and between 2011 and 2040 (future).

HESSD
12, 3787–3846, 2015

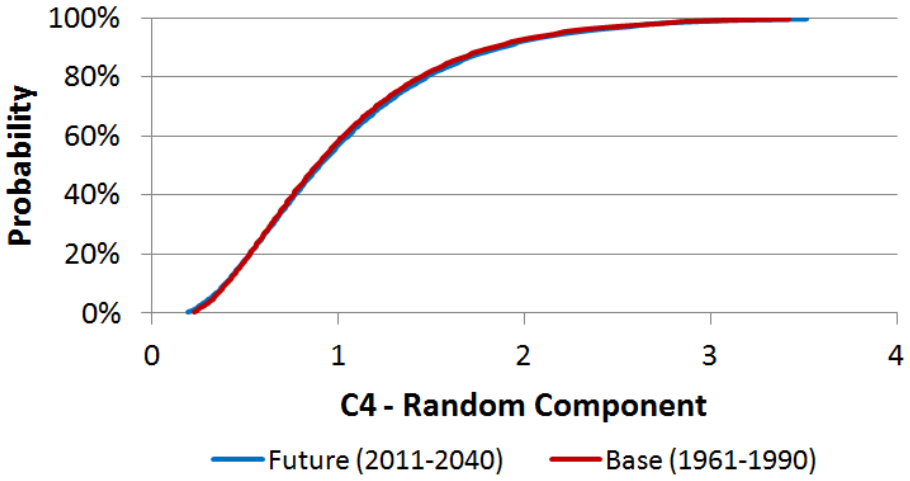

Figure 14. Adjustment of the Gamma distribution for the modeling of the random component in a low flow situation, C3(t) less than 1, for the base and future periods.

HESSD
12, 3787–3846, 2015

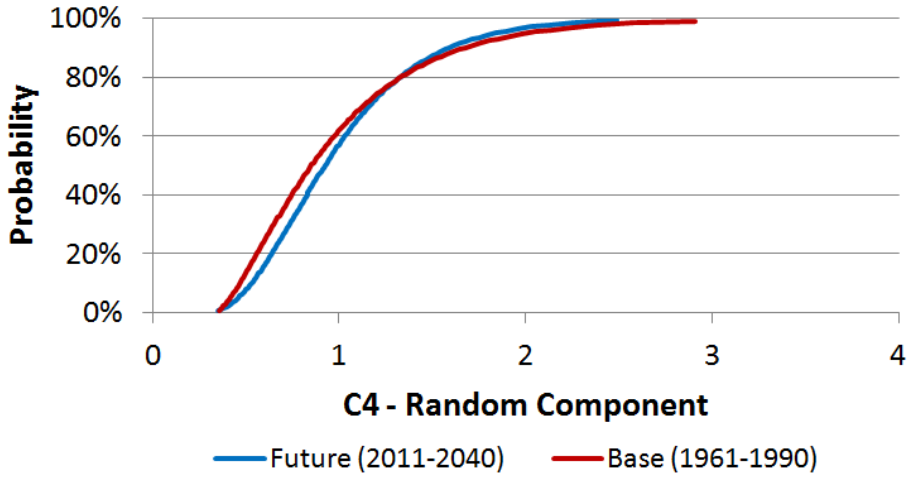

Figure 15. Adjustment of the Gamma distribution for the modeling of the random component in a high flow situation, C3(t) higher than 1, for the base and future periods.

HESSD
12, 3787–3846, 2015